Investigating the Effect of miR-145-5p Inhibition with an Antisense Oligonucleotide on Experimental Autoimmune Encephalomyelitis

Kelsea McKay

This thesis is submitted in partial fulfillment of the requirements for the Master of Science degree in Cellular and Molecular Medicine

Department of Cellular and Molecular Medicine
Faculty of Medicine
University of Ottawa

Supervisor: Dr. Rashmi Kothary

Table of Contents

Abstract

Multiple Sclerosis (MS) is a chronic, inflammatory disease of the central nervous system. MS is caused by the immune-mediated destruction of myelin and oligodendrocytes, resulting in demyelination and neurodegeneration. The microRNA miR-145-5p has been demonstrated to be upregulated in MS lesions. Our lab has previously shown that dysregulation of miR-145-5p can interfere with oligodendrocyte differentiation in mice and that knockout of miR-145-5p protects mice from experimental autoimmune encephalomyelitis (EAE), a model for MS. The objective of this study is to determine if inhibition of miR-145-5p with an antisense oligonucleotide (ASO) is sufficient to protect mice from EAE. Female mice were induced with EAE and then treated with a control or miR-145 ASO at the onset of disease. We evaluated disease progression by monitoring clinical severity, and evaluating molecular and structural characteristics of EAE by RT-qPCR, histology, immunohistochemistry and electron microscopy. We have shown that the miR-145 ASO reduced miR-145-5p expression in the lumbar spinal cord, spleen and thymus following EAE induction. Treatment with the miR-145-5p ASO resulted in improved clinical severity of EAE, reduced neuroinflammation and increased myelination. Inhibition of miR-145-5p may represent a novel treatment for MS.

Acknowledgements

I would like to thank my supervisor Dr. Rashmi Kothary for his guidance and support throughout my time in the lab. I would like to thank the entire Kothary lab for their support, encouragement and feedback. In particular, I would like to thank Dr. Samantha Kornfeld and Dr. Sarah Cummings for their mentorship over the years, and Yves De Repentigny for his contributions to the TEM portion of this thesis. I would also like to thank my Thesis Advisory Committee members, Dr. David Picketts and Dr. Diane Lagace, for their time, guidance and feedback in regard to this project. Finally, I would like to thank my parents Jennifer and Bruce, sister Hayley and partner Kyle for their endless love, support and encouragement.

List of Tables

List of Figures

List of Abbreviations

Actb – actin beta

Ago2 – argonaute-2

APC – antigen-presenting cell

ASO – antisense oligonucleotide

BBB – blood brain barrier

BSCB – blood spinal cord barrier

Ccl5 – C-C motif ligand-5

CFA – complete Freund's adjuvant

CNS – central nervous system

CSF - cerebrospinal fluid

CSPG – chondroitin sulphate proteoglycan

Cxcl1 – C-X-C motif chemokine ligand 1

DC - dendritic cell

DMD – Duchenne muscular dystrophy

DMT - disease-modifying therapy

dNTP – deoxynucleotide triphosphate

EAE – experimental autoimmune encephalomyelitis

EBV – Epstein-Barr virus

ECM - extracellular matrix

GFAP – glial fibrillary acidic protein

H&E – hematoxylin and eosin

Hes5 – Hes family BHLH transcription factor 5

Iba1 – ionized calcium-binding adapter molecule 1

IFNγ – interferon gamma

IGF1 – insulin-like growth factor 1

Il1β – interleukin 1 beta

Il6 – interleukin 6

KO - knockout

LINGO-1 – leucine rich repeat and immunoglobin-like domain-containing protein 1

MAG – myelin associated glycoprotein

MBP – myelin basic protein

miRISC – microRNA induced silencing complex

miRNA – microRNA

MOG – myelin oligodendrocyte glycoprotein

mRNA – messenger RNA

MS – multiple sclerosis

MYRF – myelin gene regulatory factor

NFκB - nuclear factor kappa-light-chain enhancer of activated B cells

Nurr1 - nuclear receptor related 1

OL – oligodendrocyte

OPC – oligodendrocyte progenitor cell

PBMC - peripheral blood mononuclear cells

PDGFRα – platelet-derived growth factor alpha

PMP22 – peripheral myelin protein 22

Ppia – peptidylprolyl isomerase A

PPMS – primary progressive multiple sclerosis

Pre-miRNA - precursor miRNA

pri-miRNA – primary miRNAs

PSA-NCAM – polysialylated neural adhesion molecule

PTX – pertussis toxin

Rho/ROCK – Rho/Rho-associated coiled-coil containing protein kinase

RNA – ribonucleic acid

RRMS – relapsing-remitting multiple sclerosis

RT-qPCR – real time quantitative polymerase chain reaction

SC – spinal cord

SMA – spinal muscular atrophy

Sox6 – SRY-box transcription factor 6

SPMS – secondary progressive multiple sclerosis

TEM – transmission electron microscopy

TGF- β1 – transforming growth factor beta 1

Th1 – T helper cell 1

Th17 – T helper cell 17

TNFα – tumor necrosis factor alpha

Twist1 - Twist related protein 2

UTR - untranslated region

1. Introduction

1.1 Multiple Sclerosis

Multiple sclerosis (MS) is an inflammatory disease of the central nervous system (CNS), resulting in neurological dysfunction (Dendrou et al., 2015). MS is characterized by the immune-mediated destruction of myelin, the insulating material surrounding neurons, resulting in the formation of demyelinating lesions (Franklin and Ffrench-Constant, 2008). These lesions lead to physical and cognitive impairments, including fatigue, limb weakness, reduced coordination, altered sensations and visual problems (Noseworthy et al., 2009).

Prevalence and Etiology

Globally, there are approximately 2.8 million people with MS and the number has increased by 30% since 2013 (Gilmour et al., 2018). The regions with the highest rates of MS include North America, northern Europe, Australia and New Zealand (Walton et al., 2020). The prevalence of MS increases in proportion to distance from the equator with the furthest regions having the highest prevalence of the disease. Canada has one of the highest rates of MS with approximately 90,000 Canadians being affected by the disease (Government of Canada, 2018). In Canada, MS is most often diagnosed between the ages of 20-49 and is three times more common in females than males (Orton et al., 2006; Government of Canada, 2018).

The etiology of MS is not fully understood, but there are both genetic and environmental factors associated with an increased risk of MS. As previously mentioned, a greater distance from the equator is correlated with an increased risk of developing MS (Simpson et al., 2011; Walton et al., 2020). Two potential explanations for this phenomenon are

a reduction in ultraviolet rays and a reduction in Vitamin D exposure (Duan et al., 2014; Ostkamp et al., 2021). Other environmental factors associated with an increased risk of MS are Epstein-Barr virus (EBV) infection, smoking and obesity (Hedström et al., 2012; Alfredsson and Olsson, 2019; Jacobs et al., 2020).

MS has also been demonstrated to have a genetic component, as seen in twin and family studies (O'Gorman et al., 2013). Individuals with a first-degree relative with MS have a slightly higher risk of developing MS than the general population. While there is no specific gene that can predict whether an individual will develop the disease, gene variations associated with an increased risk of MS have been shown to be involved in immune regulation (Hollenbach and Oksenberg, 2015). As previously mentioned, females are more susceptible to developing MS than males (Orton et al., 2006). As well, females have an earlier onset of disease and more frequent relapses, but males have been shown to progress faster (Ysrraelit and Correale, 2019). The reason for these sex differences is not yet known; however, sex hormones and sex chromosomes are being evaluated as risk factors (Golden and Voskuhl, 2017). In particular, sex hormones have been shown to have differing effects on immune cells (Golden and Voskuhl, 2017; Ysrraelit and Correale, 2019). MS has a complex etiology and likely occurs based on a combination of environmental and genetic risk factors.

Classification

There are three main types of MS: Relapse-Remitting MS (RRMS), Primary-Progressive MS (PPMS) and Secondary-Progressive MS (SPMS) (Figure 1) (Katz Sand, 2015). RRMS is the most common form of MS and involves periods of clinical symptoms followed by periods of

complete or partial remission. The patient will present with cycles of disability and recovery. Progressive forms of MS involve a gradual increase in clinical symptoms without remission. SPMS may follow RRMS and involves a progressive increase in disability. Patients with PPMS show a progressive increase in disability from the time of disease onset, resulting in a gradual decrease in neurological function.

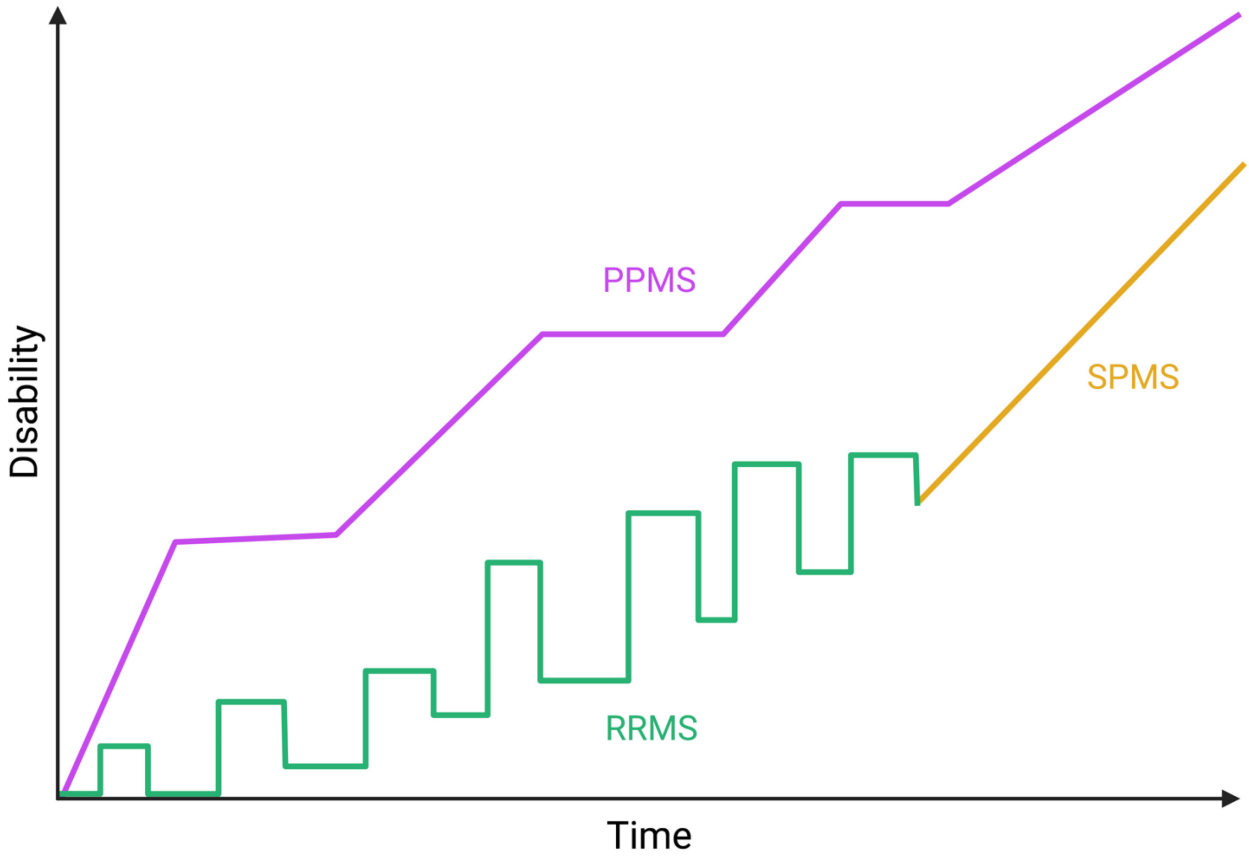

Figure 1. Classification of Multiple Sclerosis. Relapse-remitting MS (RRMS) (green) involves cycles of disability and recovery. Secondary Progressive MS (SPMS) (orange) can follow RRMS and involves a gradual increase in disability over time. Primary Progressive MS (PPMS) (purple) involves a continuous increase in disability from the start of the disease. Created with BioRender.com.

Pathology

MS lesions are most often located in the white matter of the spinal cord and brain, but can also occur in gray matter (Huang et al., 2017). Autoreactive lymphocytes (B cells and T cells) have been shown to contribute to CNS inflammation, leading to the formation of MS lesions (Hemmer et al., 2015; Langelaar et al., 2020). B cells are responsible for antibody-mediated immunity in the periphery and CNS (Hemmer et al., 2015; Michel et al., 2015). B cells mediate an immune response against myelin through the production of antibodies specific to myelin antigens. As well, B cells present myelin antigens to other immune cells and release pro-inflammatory cytokines (i.e., Il6, TNFα) (Michel et al., 2015). T cells are responsible for myelin-targeting in the CNS. Specifically, $CD4^+$ T helper cells and $CD8^+$ cytotoxic T cells have been implicated in MS pathology (Dendrou et al., 2015; Langelaar et al., 2020). T cells are activated by myelin antigens and cross the blood brain barrier (BBB), resulting in the targeting of myelin (Hemmer et al., 2015). T cells can initiate an immune response in the CNS through the direct interaction with oligodendrocytes (OLs) and neurons, and through the secretion of cytokines that can activate CNS-resident microglia and macrophages (Correale et al., 2016). These inflammatory cells lead to increased inflammation, demyelination and neurodegeneration in the CNS, resulting in clinical symptoms of MS (Lemus et al., 2018).

Treatment

Due to its complex etiology and disease course, MS is difficult to treat (Hauser and Cree, 2020). There are currently no available treatments to halt disease progression; however, disease-modifying therapies (DMTs) are being used to treat acute attacks and prolong

progression (Bross et al., 2020). There are currently 17 DMTs available in Canada (MS Society of Canada, 2021). All of the available DMTs are immunomodulatory, meaning that they work by suppressing the inflammatory response in the CNS (Bross et al., 2020). The DMTs function through various mechanisms, including the targeting of T cells, B cells, cytokines, microglia, macrophages and astrocytes (Faissner et al., 2019). These immunomodulatory therapies are all approved for treatment of RRMS and there are only a few DMTs approved for SPMS and PPMS (Baldassari and Fox, 2018). There are multiple MS treatments being studied, including monoclonal antibodies, stem cell transplants and new immunomodulatory drugs (Gholamzad et al., 2018). While these treatments target neuroinflammation, they have not been shown to promote remyelination (Cunniffe and Coles, 2021). Mechanisms to induce remyelination and provide neuroprotection are needed to improve disease outcomes (Lemus et al., 2018; Lubetzki et al., 2020; Cunniffe and Coles, 2021).

1.2 Oligodendrocytes and CNS Myelination

Oligodendrocytes (OLs) are glial cells that myelinate neurons in the CNS (Michalski and Kothary, 2015). A single OL is capable of simultaneously myelinating dozens of neurons. Myelin provides the neuron with trophic support and allows for faster electrical impulses along the axon (Kuhn et al., 2019). Myelin also functions as a protective covering of the axon; therefore, demyelination leaves the neurons vulnerable to immune cell attack. Due to the high metabolic demand of oligodendrocytes, they are vulnerable to damage in a variety of neurological diseases, including MS (Ettle et al., 2016).

OL Differentiation

OLs originate from oligodendrocyte precursor cells (OPCs) (Michalski and Kothary, 2015). During embryonic development, OPCs are derived from neural progenitor cells in the ventricular zones of the neural tube (Kuhn et al., 2019). OPCs are also generated in the adult CNS and continue to replenish lost OPCs throughout a person's life. These OPCs derive from neural stem cells from the subventricular zone (Gonzalez-Perez and Alvarez-Buylla, 2011). After being generated, OPCs migrate to both the white and gray matter of the CNS where they proliferate and eventually differentiate into myelin-producing oligodendrocytes (Michalski and Kothary, 2015).

OPCs undergo several developmental steps to differentiate into myelinating oligodendrocytes (Figure 2). The proliferative OPCs exit the cell cycle and begin to undergo morphological changes (Tiane et al., 2019). The maturing OL develops increasingly complex branches through the rearrangement of the cell's microfilaments and microtubules (Michalski and Kothary, 2015). Upon contact with neuronal axons, the OLs' myelin membrane expands and the mature OL wraps the myelin around the axon in concentric layers forming the myelin sheaths. OL differentiation is controlled by many intrinsic and extrinsic factors, including transcription factors, chromatin remodelling, signalling molecules and neuronal activity (Zuchero and Barres, 2013). Oligodendrocyte differentiation continues to occur throughout a person's life to replenish the OL population following OL death and demyelination (Dulamea, 2017). In healthy tissue, OPCs are recruited to the site of demyelination and undergo differentiation to remyelinate the denuded axons (Franklin and Ffrench-Constant, 2008). Remyelination is an important process for neuroprotection and restoration of function.

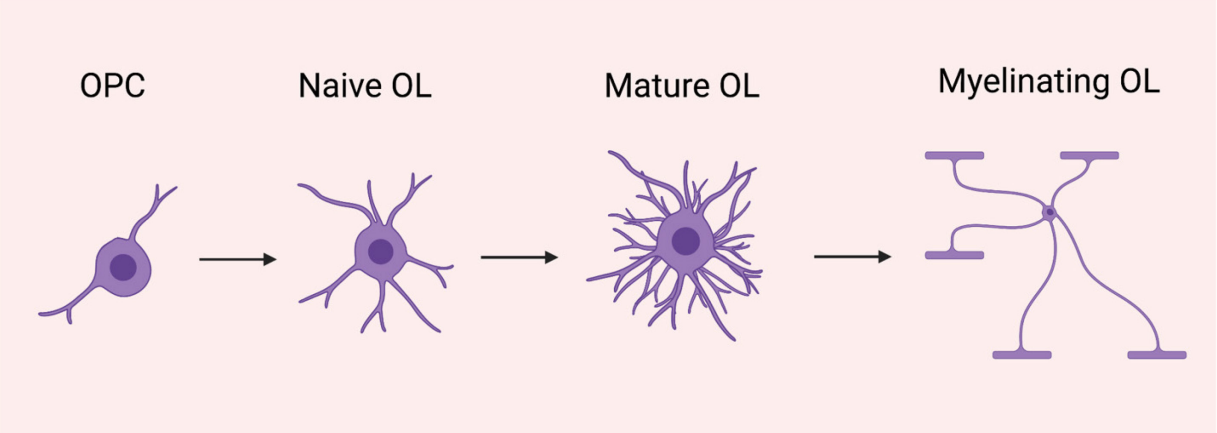

Figure 2. Oligodendrocyte Differentiation. OPCs undergo morphological changes to become myelinating OLs. The cells grow increasingly complex branches and the myelin membrane expands as they differentiate into naïve and then mature OLs. The mature OLs' branches make contact with axons and myelinate them. Created with BioRender.com.

Remyelination Failure in MS

As previously mentioned, MS involves demyelination in the CNS (Huang et al., 2017). Remyelination can occur in RRMS (Franklin and Ffrench-Constant, 2017). Following demyelination, OPCs are recruited to the MS lesion where they differentiate into OLs and remyelinate the neurons (Dulamea, 2017; Franklin and Ffrench-Constant, 2017) (Figure 3). Remyelination of the neurons in the MS lesion can lead to functional recovery. The ability to remyelinate decreases with each relapse and can eventually halt, leading to SPMS (Faissner et al., 2019). In PPMS, there is little remyelination capacity from the onset of disease. The OPCs are unable to differentiate into mature, myelinating OLs. Without remyelination, the neurons are susceptible to immune attack and neurodegeneration. Remyelination failure results in a progressive decline in disease (Lubetzki et al., 2020).

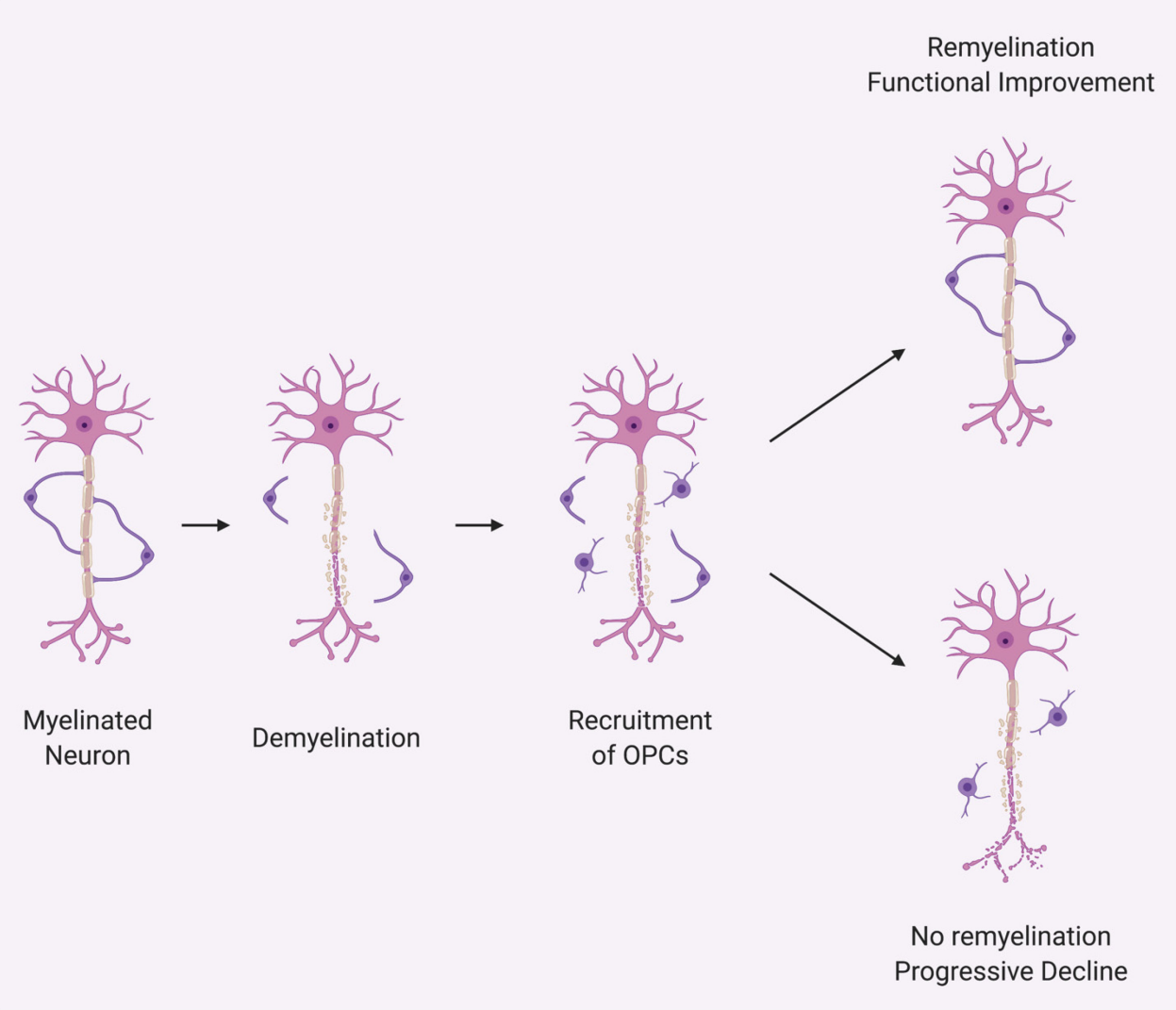

Figure 3. Remyelination in the CNS following demyelination in Multiple Sclerosis. Following demyelination, OPCs are recruited to the site of demyelination. The OPCs differentiate into OLs and remyelinate the neurons, resulting in a functional improvement. Overtime, the ability to remyelinate decreases and the OPCs are unable to differentiate into OLs, resulting in a progressive decline. Created with BioRender.com.

Remyelination failure is a common hallmark of MS. Studies have shown that there can be a failure in OPC recruitment to the site of demyelination and/or a failure in the differentiation of OPCs into mature OLs (Franklin, 2002). OPCs may not be recruited to the lesion due to the overexpression of chemorepellent molecules (i.e. Semaphorin A) or the

downregulation of chemoattractant molecules (i.e. chemokines) (Boyd et al., 2013; Watson et al., 2020). While impairments in OPC recruitment can lead to remyelination failure, it is believed that impairments in OL differentiation are the main contributor to remyelination failure since OPCs are abundant in MS lesions (Galloway et al., 2019). The environment of the MS lesion inhibits OL differentiation. Factors that have been shown to impact OL differentiation include growth factors, signalling molecules, adhesion molecules and extracellular matrix (ECM) proteins (Franklin, 2002; Harlow and Macklin, 2014; Galloway et al., 2019; Gruchot et al., 2019). Growth factors insulin-like growth factor 1 (IF1) and transforming growth factor beta 1 (TGF-β1) enhance OL differentiation; however, they have been shown to be downregulated at the MS lesion site resulting in inhibition of remyelination (Hinks and Franklin, 1999). The Notch-Jagged signalling pathway has also been shown to negatively regulate OL differentiation (Zhang et al., 2009). In the MS lesion, Jagged-1 is expressed by reactive astrocytes and binds to the Notch1 receptor on OPCs, resulting in inhibition of OL differentiation. Polysialylated neural cell adhesion molecule (PSA-NCAM) is expressed on demyelinated axons in MS lesions (Charles et al., 2002). PSA-NCAM prevents OLs from making contact with the axon; therefore, it prevents remyelination of the neuron. Chondroitin sulphate proteoglycans (CSPGs) are ECM proteins that are upregulated in MS lesions (Harlow and Macklin, 2014). Deposition of CSPGs at the site of demyelination inhibits OL process extension through the Rho/Rho-associated coiled-coil containing protein kinase (Rho/ROCK) pathway, resulting in inhibition of remyelination. Leucine rich repeat and immunoglobin-like domain-containing protein 1 (LINGO-1) has also been shown to inhibit remyelination through the Rho/ROCK pathway (Galloway et al., 2019). While inhibition of LINGO-1 improved remyelination in mouse models of MS, it has not been effective

in human clinical trials (Mi et al., 2007; Ruggieri et al., 2017). While these factors may contribute to impaired remyelination, the cause of remyelination failure in MS is not entirely known. Developing a better understanding of why remyelination fails in MS is critical to develop therapeutics to promote remyelination.

1.3 Experimental Autoimmune Encephalomyelitis

Experimental Autoimmune Encephalomyelitis (EAE) is a mouse model used in MS research (Bjelobaba et al., 2018). While other MS models are toxin-induced, EAE is induced with active immunization with myelin peptides (Constantinescu et al., 2011). In this model, mice are injected with a myelin antigen (i.e., MOG), complete Freund's adjuvant (CFA) and pertussis toxin (PTX) (Hooke Laboratories, 2008). The myelin antigens activate myelin-specific $CD4^+$ T cells, CFA induces an immune response and PTX disrupts the blood spinal cord barrier (BSCB) permitting an immune response in the spinal cord (Bennett et al., 2010; Constantinescu et al., 2011).

Following EAE induction, the myelin antigens initiate a myelin-specific immune response (Figure 4) (Robinson et al., 2014). In the periphery, the myelin antigens activate dendritic cells (DC) in the lymph nodes (Chastain et al., 2011). DCs are antigen-presenting cells (APC) that are important for adaptive immunity. DCs present the myelin antigens to naïve T cells, eliciting effector T cell differentiation. T cells specifically differentiate into myelin-specific $CD4^+$ T helper cells 1 (Th1) and 17 (Th17) (El-behi et al., 2010). Th1 and Th17 cells enter the bloodstream and cross the BSCB. T helper cells accumulate in the white matter of the CNS and are reactivated by CNS-resident APCs, resulting in the release of cytokines and recruitment of both peripheral (i.e., neutrophils, macrophages) and CNS (i.e., microglia, astrocytes, macrophages) immune cells

(Chu et al., 2018; Pierson et al., 2018). This inflammatory cascade results in the destruction of myelin and oligodendrocytes, leading to demyelination and neurodegeneration (Patel and Balabanov, 2012).

Mice with EAE exhibit increasing ascending paralysis until they reach full hind limb paralysis (Constantinescu et al., 2011). Following the peak of the disease, the mice will show partial recovery. The degree of paralysis directly reflects the extent of demyelination and inflammation in the CNS (Kipp et al., 2017). While EAE shares many traits with MS, it is not an exact replica of the disease (Bjelobaba et al., 2018). However, EAE is still the best animal model to represent the autoimmune aspect of MS, specifically RRMS.

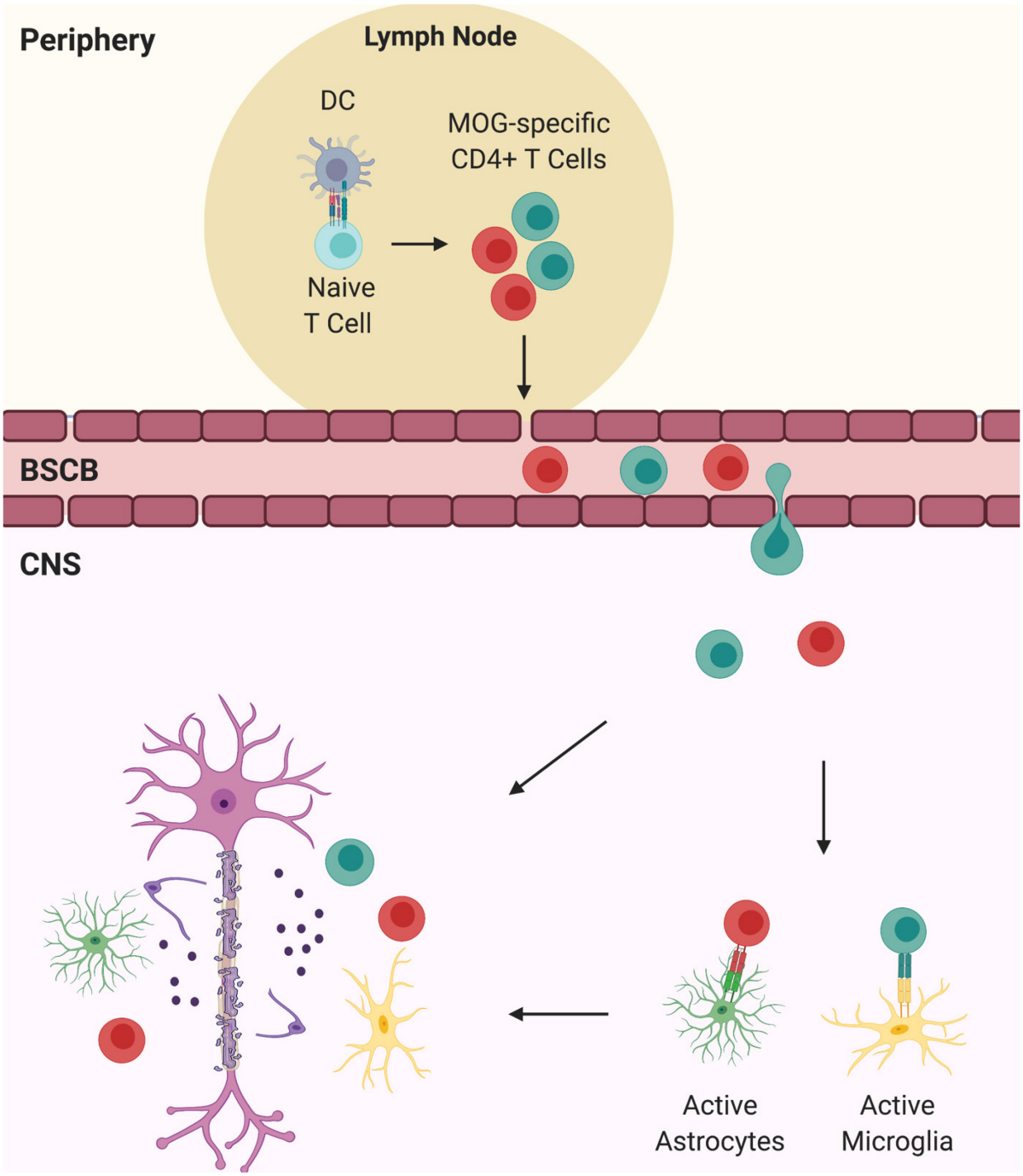

Figure 4. Pathophysiology of Experimental Autoimmune Encephalomyelitis. Following MOG-specific EAE induction, dendritic cells (DC) are activated in the lymph nodes. The DC cells present MOG antigens to naïve T cells. The T cells are activated and differentiate into MOG-specific $CD4^+$ T helper cells (Th1 and Th17). T helper cells enter the bloodstream and cross the blood spinal cord barrier (BSCB) into the central nervous system (CNS). T helper cells are reactivated when they encounter myelin antigens, resulting in the release of inflammatory cytokines, recruitment of other immune cells (i.e. microglia and astrocytes) and the destruction of myelin and oligodendrocytes. Created with BioRender.com.

1.4 MicroRNAs

MicroRNAs (miRNAs) are small, non-coding ribonucleic acids (RNAs) that regulate gene expression by post-transcriptionally silencing messenger RNAs (mRNAs) (Mohr and Mott, 2015). They regulate gene expression by inhibiting protein synthesis both directly and indirectly. The miRNA usually binds to the 3' untranslated region (UTR) of the mRNA causing inhibition of translation and/or degradation (Catalanotto et al., 2016). miRNAs are involved with many important biological processes including development, metabolism, cell-cycle control, apoptosis and cell differentiation (Lynam-Lennon et al., 2009; Shi and Jin, 2009; Chen et al., 2010; Jeker and Bluestone, 2013; Saliminejad et al., 2019). Dysregulation of miRNAs has been demonstrated in many diseases, including MS (de Faria Jr et al., 2012; Juźwik et al., 2019).

Biogenesis

miRNA biogenesis is a controlled process that begins in the nucleus (Kim, 2005; Winter et al., 2009; Krol et al., 2010; Matsuyama and Suzuki, 2020). The majority of miRNAs are generated through canonical miRNA processing (Figure 5). miRNA genes are transcribed by RNA polymerase II and the nucleotides fold upon themselves to form a hairpin structure referred to as the primary miRNA (pri-miRNA). The pri-miRNA is processed by two RNase III enzymes: Drosha and Dicer. The pri-miRNA is cleaved by the Drosha-DGCR8 nuclear microprocessor complex resulting in the formation of the precursor miRNA (pre-miRNA). The pre-miRNA is exported to the cytoplasm by the Exportin-5-Ran-GTP complex. Once the pre-miRNA is in the cytoplasm, it is cleaved by the Dicer-TRBP complex. The hairpin structure is removed resulting

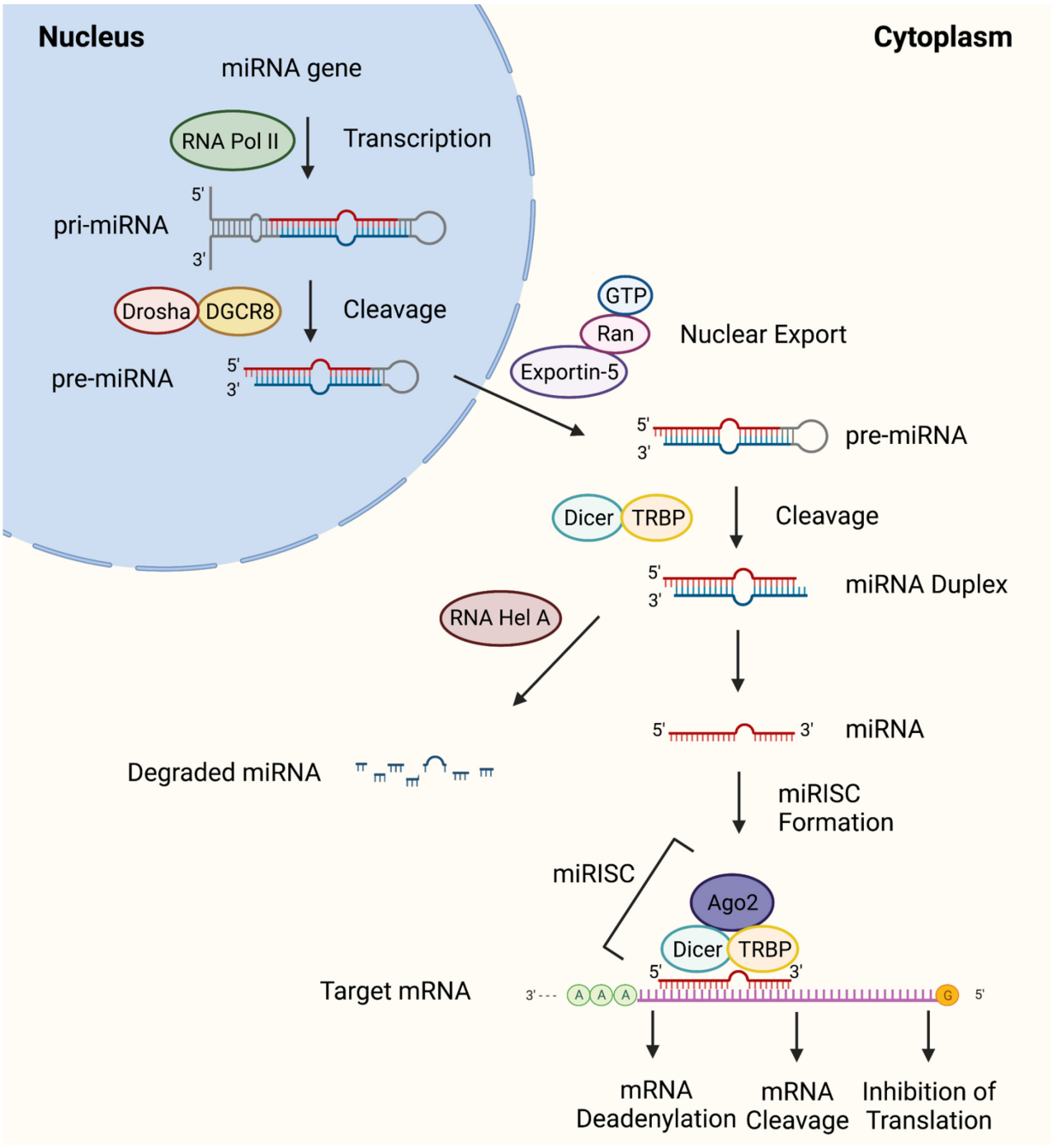

Figure 5. Canonical microRNA Processing Pathway. In the nucleus, the microRNA (miRNA) gene is transcribed by RNA polymerase II (RNA Pol II) forming the primary miRNA (pri-miRNA). The pri-miRNA is cleaved by Drosha-DGCR8 forming the pre-miRNA. The pre-miRNA is exported out of the nucleus by Exportin-5-Ran-GTP. In the cytoplasm, the stem-loop is cleaved by Dicer-TRBP forming the miRNA duplex. One strand of the miRNA duplex is degraded by RNA Helicase A (RNA Hel A) and the other strand becomes the functional miRNA. The miRNA binds to Ago2, Dicer and TRBP forming the miRNA RNA-induced silencing complex (miRISC). The miRNA guides the miRISC complex to the target RNA and silences the mRNA through mRNA deadenylation, mRNA cleavage or inhibition of translation. Created with BioRender.com.

in a miRNA duplex. Mature miRNAs are single stranded; therefore, one strand of the miRNA duplex is degraded by RNA Helicase A. The functional miRNA strand is incorporated into the miRNA RNA-induced silencing complex (miRISC). The miRISC complex is comprised of Argonaute-2 (Ago2), Dicer-TRBP and the mature miRNA. The miRNA acts as a guide for the miRISC and the miRNA binds to the target mRNA. The mRNA is silenced through three possible mechanisms: cleavage, deadenylation or inhibition of translation.

Role of miRNAs in OL Differentiation

As previously mentioned, miRNAs regulate many biological processes, including cell differentiation (Shi and Jin, 2009). miRNAs have been demonstrated to play a critical role in OL differentiation and myelination (Li and Yao, 2012). The CNS-specific conditional knockout of Dicer during late embryonic development resulted in defects in OPC expansion and OL differentiation in mice (Kawase-Koga et al., 2009). The postnatal OL-specific conditional knockout of Dicer resulted in severe OL differentiation and myelination defects, as well as neuroinflammation and demyelination (Shin et al., 2009).

Many miRNAs are differentially regulated throughout OL development (Galloway and Moore, 2016). Proliferating OPCs have high expression of miR-9, miR-125a-3p, miR-145-5p and miR-199a-5p (Lau et al., 2008; Letzen et al., 2010; Buller et al., 2012; Lecca et al., 2016; Kornfeld et al., 2021). Their expression is reduced in differentiating and mature OLs, suggesting that they control the transition of OPC to naïve OL. These miRNAs target genes involved in OL differentiation and myelin membrane compaction, including myelin gene regulatory factor (MYRF), myelin oligodendrocyte glycoprotein (MOG) and peripheral myelin protein 22 (PMP22)

(Lau et al., 2008; Letzen et al., 2010; Kornfeld et al., 2021). Overexpression of these miRNAs and subsequent repression of their targets would inhibit OL differentiation. There is an upregulation of miR-23a, miR-138, miR-146a, miR-219 and miR-338 as OLs differentiate and become mature, myelinating OLs (Lin and Fu, 2009; Dugas et al., 2010; Li et al., 2019; Zhang et al., 2019). These miRNAs likely target genes involved in OPC proliferation and inhibition of differentiation, including platelet-derived growth factor alpha (PDGFRα), SRY-box transcription factor 6 (Sox6) and Hes family BHLH transcription factor 5 (Hes5). These genes keep OPCs in a proliferative state; therefore, miRNA-mediated inhibition of these genes would allow for OL differentiation. miRNAs are important for controlling OL differentiation and their dysregulation could lead to OL defects.

Role of miRNAs in CNS Inflammation

miRNAs play an important role in the development and regulation of the immune system. T cell-specific knockout of Dicer resulted in deficits in T cell development, differentiation and cytokine production (Cobb et al., 2005; Muljo et al., 2005). B cell-specific knockout of Dicer resulted in a reduction in the number of B cells and impaired antibody production (Koralov et al., 2008). These studies demonstrate that miRNAs are important for the regulation of lymphocyte development and function.

Many miRNAs have been shown to have important roles in the regulation of the immune system (Jeker and Bluestone, 2013). miR-17-92 cluster and miR-155 have been shown to promote T cell differentiation (O'Connell et al., 2010; Wu et al., 2012). miR-17-92 promotes T cell proliferation and expansion (Wu et al., 2012). Overexpression of miR-155 is seen in EAE and

knockout of miR-155 resulted in a reduction in Th1 and Th17 cell responses, suggesting that miR-155 is essential for T cell development (Murugaiyan et al., 2011). miR-155 is also important for B cell differentiation (Mahesh and Biswas, 2019). Knockout of miR-155 results in a reduction in the number of B cells and impaired B cell function. Other miRNAs that promote B cell development include miR-19b, miR-25, miR-93, miR-106b and miR-181a (Sievers et al., 2012; Borbet et al., 2021). While the role of miRNAs in CNS inflammation is not fully known, it is evident that miRNAs are required for development and regulation of the immune system; therefore, miRNA dysregulation could lead to impaired inflammatory processes.

miRNA Dysregulation in MS

Since miRNAs are important for OL differentiation and CNS inflammation, it is not surprising that miRNA dysregulation is seen in MS (de Faria Jr et al., 2012). Many miRNAs are differentially expressed in people with MS and healthy controls. miRNA profiles derived from whole blood and peripheral blood mononuclear cells (PBMCs) show that you can distinguish between samples from people with MS and healthy controls based on the miRNA expression pattern (Keller et al., 2009; Otaegui et al., 2009). As well, you can differentiate between people with RRMS in relapse and in remission based on expression of several miRNAs (Otaegui et al., 2009). One miRNA that has been shown to distinguish people with MS from healthy controls is miR-145-5p (Keller et al., 2009). miR-145-5p is overexpressed in whole blood, PBMCs and MS lesions (Keller et al., 2009; Tripathi et al., 2019). When examining expression of miRNAs in active MS lesions compared to healthy white matter, multiple miRNAs were dysregulated (Junker et al., 2009; Tripathi et al., 2019). miR-219 and miR-338 were downregulated and miR-

23a and miR-155 were upregulated in MS lesions. These findings suggest that miRNAs may have potential as novel biomarkers and targets for treatment in MS.

miR-145-5p in OL Differentiation and Animal Models of MS

As previously mentioned, miR-145-5p is overexpressed in MS patients. The role of miR-145-5p in MS pathology is not entirely known; however it has been implicated in OL differentiation (Letzen et al., 2010). miR-145-5p is highly expressed in OPCs and is downregulated as OLs differentiate, suggesting that it regulates the transition of OPC to OL. Predicted targets of miR-145-5p include MYRF and other genes involved in OL differentiation; therefore, miR-145-5p overexpression would lead to impaired OL development (Emery et al., 2009; Letzen et al., 2010).

Our lab has previously studied the role of miR-145-5p in OL differentiation in primary rat OL cultures *in vitro* (Kornfeld et al., 2021). Overexpression of miR-145-5p resulted in impaired OL differentiation, as demonstrated with a reduction in the number of mature OLs, less complex branching, decreased myelin membrane area and reduced expression of myelin genes, including myelin-associated glycoprotein (MAG), myelin basic protein (MBP) and MYRF. The knockdown of miR-145-5p resulted in improved OL differentiation, as demonstrated with an increase in the number of mature OLs, more complex branching, increased myelin membrane area and increased expression of MAG and MYRF. These results suggest that miR-145-5p is important for maintaining OPCs in a proliferative state and preventing premature OL differentiation.

Our lab has also investigated the effect of miR-145-5p knockout (KO) in mouse models of MS. In the cuprizone toxin-induced mouse model, miR-145-5p KO improved remyelination following chronic cuprizone exposure (Kornfeld *et al*., unpublished). There was a significant increase in the number of myelinated axons and the thickness of the corpus callosum. In the EAE mouse model, miR-145-5p KO resulted in reduced clinical severity of EAE, as demonstrated with delayed disease onset, delayed onset of paralysis, and reduced duration of paralysis (Kornfeld *et al*., unpublished). There was also a significant increase in myelination and a significant reduction in inflammation in the lumbar spinal cord. These results suggest that miR-145-5p is important for OL differentiation and remyelination, as well as CNS inflammation.

Inhibition of miRNAs with Antisense Oligonucleotides

Antisense oligonucleotides (ASOs) are synthetic, single-stranded oligonucleotides designed to bind to specific RNAs and alter their function (Rinaldi and Wood, 2017). ASOs bind to the target RNA through complimentary base pairing and deactivate it through inhibition, degradation or alternative splicing depending on the type of RNA and target sequence. The first generation of ASOs had limited therapeutic potential because they were rapidly degraded by exonucleases (Frazier, 2015). Over the years, much progress has been made in the development of ASOs. Current ASOs have base and backbone modifications, allowing them to have a higher binding affinity and evade degradation (Bennett, 2019). There are currently several oligonucleotide therapies, including ASOs, approved for the treatment of human diseases, including Eteplirsen and Golodirsen for Duchenne muscular dystrophy (DMD), and Nusinersen for spinal muscular atrophy (SMA) (Dhuri et al., 2020; Hammond et al., 2021).

While early ASOs were designed to bind to mRNAs, there are now ASOs designed to target miRNAs (Bajan and Hutvagner, 2020). As previously mentioned, the miRNA joins the miRISC complex and binds to the mRNA preventing its translation (Figure 6a) (Matsuyama and Suzuki, 2020). The miRNA ASO binds to its target miRNA, preventing the miRNA from being incorporated into the miRISC complex and allowing translation to occur (Figure 6b) (Broderick and Zamore, 2011). miRNA inhibition with an ASO may represent a novel therapeutic strategy for human diseases, including MS (Sun et al., 2018).

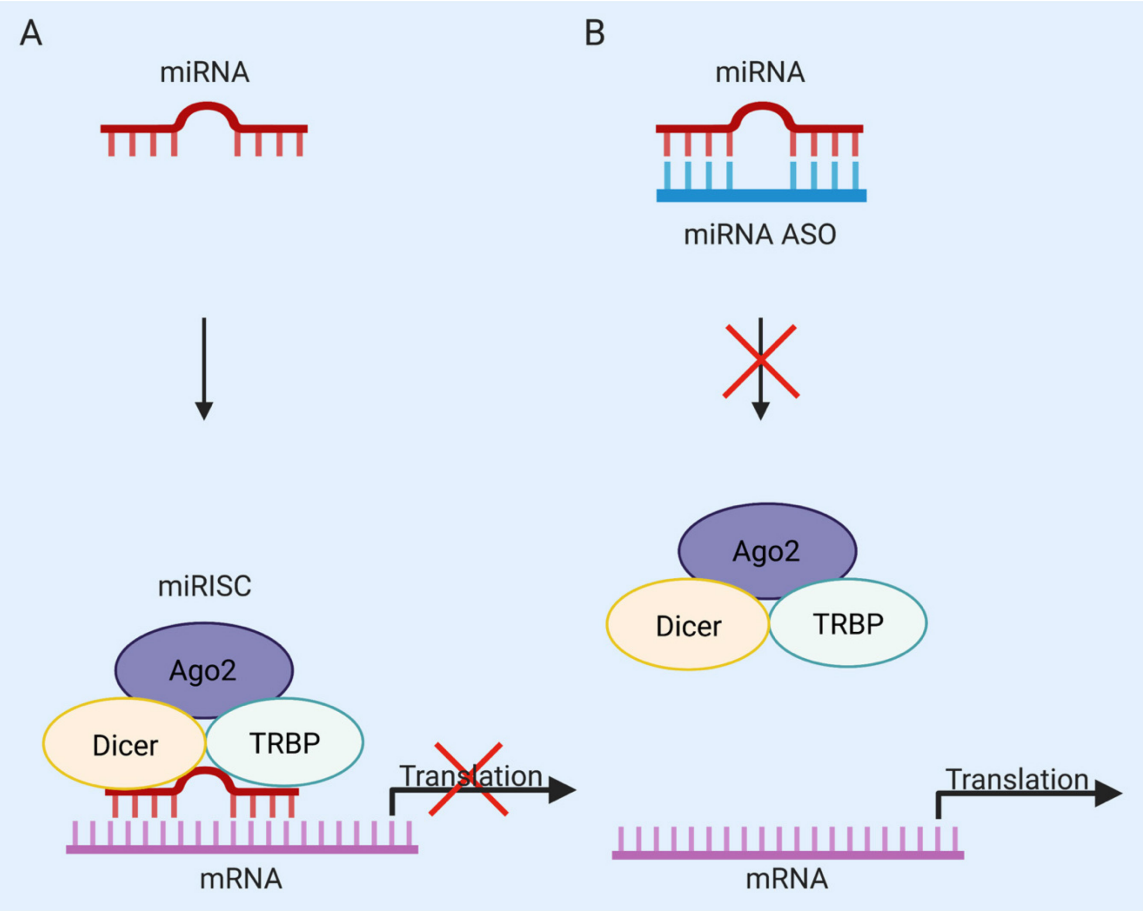

Figure 6. Inhibition of microRNAs with Antisense Oligonucleotides. A) The mature miRNA is incorporated into the miRISC complex which binds to the target mRNA and inhibits its translation. B) The miRNA antisense oligonucleotide (ASO) binds to the mature miRNA and prevents it from being incorporated into the miRISC complex. The miRNA does not bind to the target mRNA and its translation can occur. Created with BioRender.com.

1.5 Research Methods and Aims

Our lab has demonstrated that KO of miR-145-5p leads to improvements in clinical severity, loss of myelin and immune cell infiltration in mice with EAE. While the miR-145-5p KO mouse model allowed us to develop a better understanding of the role of miR-145-5p in remyelination and CNS inflammation, miR-145-5p inhibition at disease onset is necessary to investigate the therapeutic potential of miR-145-5p. The use of an ASO to inhibit miR-145-5p at EAE onset would allow us to investigate how miR-145-5p knockdown following EAE induction impacts clinical severity, inflammation and myelination. We hypothesize that inhibition of miR-145-5p at onset of EAE with an ASO would improve clinical severity, reduce inflammation and improve remyelination.

Aims:

1. Optimize the use of an ASO to knockdown miR-145-5p in CNS and lymphoid tissues of naïve mice.
2. Evaluate the effect of miR-145 ASO treatment at EAE onset on clinical severity of disease.
3. Investigate molecular and cellular changes in CNS and lymphoid tissues of mice treated with miR-145 ASO at EAE onset.

1. Materials and Methods

2.1 Animals

C57BL/6 mice (Charles River Laboratories) were treated with an ASO and/or induced with EAE when they reached 10-13 weeks of age. Mice were sacrificed at various timepoints following treatment for *in vivo* analyses. All mice were maintained with a 12 h light-dark cycle and *ad libitum* access to food and water. All animal experiments were approved by the University of Ottawa Animal Care Committee and in accordance with the guidelines of the Canadian Council for Animal Care.

2.2 Antisense Oligonucleotide Optimization

Mice were injected with various doses (20-100 µg/mouse) of the mirVana (Fisher Scientific, 4464088) or 20 µg/mouse of the custom *in vivo* miRCURY (Qiagen, 339203) negative control and miR-145-5p ASOs by tail vein injection. Mice were sacrificed 24 h following administration of the ASOs, and spleen, thymus, lumbar spinal cord and brain tissue were collected for RNA isolation and RT-qPCR to measure miR-145-5p expression.

2.3 Experimental Autoimmune Encephalomyelitis Induction

EAE was induced in female mice using a kit produced by Hooke Laboratories and according to their protocol (NC0425310) (Hooke Laboratories, 2008). The mice were subcutaneously injected on both the upper and lower back with 100 µL of the prepared MOG_{35-55}/CFA emulsion and intraperitoneally injected with 100 ng PTX (Sigma-Aldrich, P2980) on day 0. A second injection of PTX was administered on day 1 and the mice were not disturbed until

day 7 to allow EAE induction to occur. Mice were scored daily and weighed semi-daily from day 7 until day 30. EAE is scored based on manufacturer's guidelines: 0.0 = no changes to motor function; 0.5 = partial tail paralysis; 1.0 = complete tail paralysis; 1.5 = tail paralysis and hind leg inhibition; 2.0 = tail paralysis and hind leg weakness; 2.5 = tail paralysis and dragging of at least one hind leg; 3.0 = tail paralysis and paralysis of hind legs; 3.5 = tail paralysis, hind leg paralysis and inability to right itself or flattening of hind quarters; 4.0 = tail paralysis, hind leg paralysis and partial front leg paralysis; 4.5 = tail paralysis, hind leg paralysis and front leg paralysis; 5.0 = death. No mouse exceeded a score of 3.5. Mice were treated with the control or miR-145 ASO once they reached an EAE score > 0.0 and were sacrificed for tissue collection at onset, peak and chronic timepoints. Onset was 24 h following ASO administration, peak was defined as the time when the mice reach an EAE score $\geq$3.0 and chronic is arbitrarily set at day 30. The control animals are naïve, female mice 10-13 weeks of age.

2.4 RNA Isolation and RT-qPCR

RNA was extracted using the RNeasy Mini kit (Qiagen, 74106) according to the manufacturer's protocol. The kit includes Qiagen's proprietary buffers "RLT", "RW1" and "RPE". Briefly, 30 µg of flash-frozen tissue (spleen, thymus, lumbar spinal cord) was homogenized in 350-600 µL of RLT lysis buffer and then centrifuged for 3 min at maximum speed. The supernatant was transferred to a new centrifuge tube, mixed with an equal amount of 70% ethanol with RNase-free water (350-600 µL), transferred to the RNeasy spin column and centrifuged for 25 s at maximum speed. The eluate was discarded and 700 µL Buffer RW1 was added to spin column. The tube was centrifuged for 25 s at maximum speed and the eluate was

discarded. The sample was washed with 500 µL Buffer RPE, centrifuged for 25 s at maximum speed and the eluate was discarded. Next, the sample was washed with 500 µL Buffer RPE, centrifuged for 2 min at maximum speed and the eluate was discarded. The column was moved to a new collection tube and centrifuged for 1 min at full speed. Finally, the spin column was transferred to an RNase-free micro-centrifuge tube and RNA was eluted in 30-60 µL RNase-free water by centrifuging the tube for 1 min at maximum speed. The RNA was stored at -80°C until cDNA synthesis.

For miRNA analysis, cDNA was synthesized by combining 300 ng total RNA with 1 µL of the appropriate 1250 nM stem-loop primer (Table 1) and enough RNase-free water to get a volume of 10 µL. The sample was incubated for 5 min at 95°C, 5 min at 60°C and then immediately centrifuged and placed on ice for at least 1 min. Reverse transcription was performed using the M-MLV Reverse Transcription kit (Invitrogen, 28025013). One µL M-MLV Reverse Transcriptase, 8 µL reverse transcription buffer (4x First Strand Buffer, 2x dithiothreitol, 1x dNTPs (25 µM)) and 6 µL RNase-free water were added to the sample to obtain a volume of 25 µL. An Eppendorf Mastercycler was used for the reaction with the following protocol: 16°C for 30 min; 60 cycles of 20°C for 30 s, 42°C for 30 s and 50°C for 1 s; 85°C for 5 min.

Table 1. Primer Sequences for miRNA cDNA Synthesis

Primer	Sequence (5’ - 3’)
miR-145-5p stem-loop	CTCACAGTACGTTGGTATCCTTGTGATGTTCGATGCCATATTG TACTGTGAGAGGGATTC
snU6 stem-loop	CTCACAGTACGTTGGTATCCTTGTGATGTTCGATGCCATATTG TACTGTGAGAAAAATATGGAACGCTT

For miRNA RT-qPCR, each reaction contained 4 µL cDNA, 12.5 µL SsoAdvanced Universal SYBR Green Supermix (Bio-Rad, 1725275), 0.8 µL forward primer, 0.8 µL reverse primer and 6.9 µL RNase-free water. All primers for miRNA cDNA synthesis (Table 1) and RT-qPCR (Table 2) were obtained from AlphaDNA. RT-qPCR was performed using a Bio-Rad CFX Connect and the following protocol: 95°C for 10 min; 40 cycles of 95°C for 15 s and 60°C for 1 min. All samples were run in technical triplicates. Fold changes were calculated using the ΔΔCt method and normalized to snU6.

Table 2. Primer Sequences for miRNA RT-qPCR

Primer	Sequence (5' - 3')
miR-145-5p forward	ACACTCCAGCTGGGGTCCAGTTTTCCCAGG
snU6 forward	ACACTCCAGCTGGGGTGCTCGCTTCGGCAGCACATA
Universal reverse	CTCACAGTACGTTGGTATCCTTGTG

For mRNA analysis, total cDNA was synthesized using the RT^2 First Strand Kit, including proprietary solutions Buffer GE, Buffer BC3, Control P2 and RE3 Reverse Transcriptase Mix (Qiagen, 330401). First, genomic DNA was eliminated by combining 200 ng RNA with 2 µL Buffer GE and enough RNase-free water to get a volume of 10 µL. The mixture was incubated for 5 min at 42 °C and then immediately placed on ice for at least 1 min. Next, reverse transcription was executed by adding 4 µL 5x Buffer BC3, 1 µL Control P2, 2 µL RE3 Reverse Transcriptase Mix and 3 µL RNase-free water. The RNA samples were incubated for 15 min at 42°C and 5 min at 95°C.

The cDNA samples were diluted by adding 91 µL RNase-free water and the cDNA samples were kept at -20°C until RT-qPCR.

For mRNA qRT-PCR, each reaction contained 4 µL total cDNA, 10 µL SsoAdvanced Universal SYBR Green Supermix (Bio-Rad, 1725275), 1 µL PrimePCR pre-optimized forward/reverse primers (Bio-rad, 10025636) and 5 µL RNase-free water. RT-qPCR was performed using a Bio-Rad CFX Connect and the following protocol: 95°C for 2 min; 40 cycles of 95°C for 5 s and 60°C for 30 s; 65°C to 95°C in increments of 0.5°C for 5 s. All samples were run in technical triplicates. Fold changes were calculated using the ΔΔCt method and normalized to actb and ppia.

2.5 Histology and Immunohistochemistry

Mice were sacrificed at naïve, onset, peak and chronic timepoints, as previously described. Whole spinal columns were dissected and placed in formalin for 48 h at 4°C. The spinal columns were placed in 70% ethanol for 24 h at 4°C. The spinal cords were then removed from the spinal columns and the lumbar spinal cords were isolated. The samples were placed in 70% ethanol at 4°C until they were sent to the Louise Pelletier Histology Core Facility (Department of Pathology and Laboratory Medicine, University of Ottawa) for further processing. All spinal cords were embedded in paraffin with a LOGOs microwave hybrid tissue processor and lumbar spinal cord cross-sections were cut by microtome at a thickness of 5 µm, before being mounted on slides.

For histology, sections were stained at the Louise Pelletier Histology Core Facility (Department of Pathology and Laboratory Medicine, University of Ottawa). A Leica ST5010

Autostainer XL was used to stain lumbar spinal cord sections with hematoxylin and eosin (H&E) and a Leica CV5030 Glass Coverslipper was used to place coverslips on stained sections.

Sections were deparaffinized and rehydrated prior to immunohistochemistry. First, the slides were incubated at 59^{o}C for at least 30 min. Slides were then incubated in the following solutions: 100% Hemo-D (Histo-Clear) for 3 x 5 min, 50% Hemo-D/50% ethanol for 2 x 3 min, 100% ethanol for 2 x 3 min, 95% ethanol for 3 min, 70% ethanol for 3 min, 50% ethanol for 3 min and then rinsed twice with water. For Iba1 staining, antigen retrieval was performed by incubating the slides in Tris EDTA buffer (pH 9.0) for 20 min at approximately 100^{o}C using a vegetable steamer. Slides were then rinsed with water for 10 min. The slides were dried following rehydration or antigen retrieval, and then the sections were washed 3 x 5 min in PBS. The sections were permeabilized in 0.5% Triton-x-100 in PBS for 20 min and then washed 3 x 5 min in PBS, before being blocked for 1 h at room temperature in a blocking solution (1% bovine serum albumin, 10% goat serum, 0.2% Triton-x-100 in PBS). The slides were incubated overnight at 4^{o}C in the antibody solution (1% bovine serum albumin, 1% goat serum, 0.2% Triton-x-100 in PBS) containing the appropriate primary antibody at the following concentrations: GFAP: 1:1000 (Agilent, Z033429-2), Iba1: 1:1000 (Abcam, ab178846), MBP: 1:100 (Serotech, MCA409S). Sections were washed 3 x 5 min in PBS and then incubated for 1 h at room temperature in the antibody solution (1% bovine serum albumin, 1% goat serum, 0.2% Triton-x-100 in PBS) containing the appropriate AlexaFluor secondary antibody. The sections were washed for 5 min in PBS, stained with DAPI (1:1000 in PBS) for 5 min and then rinsed 3 x 5 min in PBS. The slides were dried and then Dako fluorescent mounting medium was added directly to the sections before a coverslip was applied.

2.6 Transmission Electron Microscopy

Mice were anesthetized via intraperitoneal injection of Tribromoethanol (Avertin) and perfused transcardially with 5 mL of PBS followed by 10-20 mL of Karnovsky's fixative (4% paraformaldehyde (PFA), 2% glutaraldehyde and 0.1 M sodium cacodylate in PBS, pH 7.4). The spinal cords were extracted and fixed overnight (or until processed) at 4^{o}C in the same fixative. After fixation, lumbar spinal cord regions were dissected and cut under a stereomicroscope into straight segments of 1 mm of length. Segments were subsequently washed twice in 0.1 M sodium cacodylate buffer for 1 h and left in sodium cacodylate buffer overnight at room temperature. Specimen were post-fixed with 1% osmium tetroxide in 0.1 M sodium cacodylate buffer for 1 h at room temperature and were then washed in distilled water 3 x 5 min. Samples were dehydrated twice for 20 min for each step in a graded series of ethanol (30%, 50%, 70%, 85%, 95%), followed by 2 x 30 min in 100% ethanol, 2 x 15 min in 50% ethanol/50% acetone and 2 x 15 min in 100% acetone. Specimens were then infiltrated in 30% Spurr resin/acetone for 20 min and once for 15 h (overnight), then in 50% Spurr resin/acetone for 6 h and in fresh 100% Spurr resin overnight. Spurr resin was changed twice a day for three days at room temperature. All infiltration steps were performed on a rotator at low speed. Finally, segments were embedded in fresh liquid Spurr resin and oriented inside the molds and then polymerized overnight at 70^{o}C. Ultrathin sections (80 nm) were collected onto 200-mesh copper grids and stained with 2% aqueous uranyl acetate and with Reynold's lead citrate.

2.7 Imaging and Quantification

Histology and Immunohistochemistry sections were imaged at a magnification of 10x with a Zeiss AxioScan slide scanner with a Colibri 7 camera and Zen 2.6 slidescan software. Electron micrographs were taken with a Transmission Electron Microscope (TEM) at a magnification of 10,000X (TEM Hitachi 7100). All images were blinded and then analyzed with ImageJ. Total spinal cord area and nucleus-dense area were measured to calculate percent infiltrated area in H&E images. For GFAP analysis, $GFAP^+$ cells were counted over the entire section. For Iba1 analysis, $Iba1^+$ cells were counted in the parenchyma, excluding areas of dense cellular infiltration. To calculate percent myelination area, all MBP images were set to the same threshold value and the "Analyze Particles" plug-in was used to produce MBP traces. For the TEM analysis, all myelinated axons were counted in images taken at 10 000X.

2.8 Statistical Analysis

Prism 6 GraphPad software was used for all statistical analyses. Two-tailed t-tests were used for pair-wise comparisons and two-way ANOVAs were used for >2 comparisons. Mantel-Cox testing was used to analyze Kaplan-Meier curves. Chi-square testing was used for categorical variables. Data is expressed as mean $\pm$ SEM unless otherwise indicated. For all analyses, $p<0.05$ was considered statistically significant. Asterisks represent level of significance as follows: *=$p<0.05$, **=$p<0.01$, ***=$p<0.001$, ****=$p<0.0001$.

2. Results

3.1 A single miR-145 ASO administration reduced miR-145-5p levels in lymphoid but not CNS tissue of naïve mice

We first optimized the use of an ASO to knockdown miR-145-5p levels in both lymphoid and CNS tissues. Naïve mice were injected with the Fisher Scientific control or miR-145 ASO at various doses. The mice were sacrificed 24 h following ASO treatment, and the spleen and lumbar spinal cord were dissected. Relative level of miR-145-5p was analyzed by RT-qPCR. The miR-145 ASO did not significantly reduce miR-145-5p levels in the spleen or lumbar spinal cord at any of the doses used (Figure 7).

Since the Fisher Scientific ASO did not knockdown miR-145-5p levels, we decided to test an ASO from a different commercial supplier. Naïve mice were injected with the Qiagen control or miR-145 ASO at a dose of 20 µg/mouse. Spleen, thymus, lumbar spinal cord and brain tissue was dissected 24 h following ASO treatment, and the relative level of miR-145-5p was analyzed by RT-qPCR. There was a significant reduction in miR-145-5p in the spleen and a trend towards a reduction in the thymus (Figure 8A). There was no reduction in miR-145-5p in the lumbar spinal cord or brain tissue.

We wanted to assess the longevity of miR-145-5p knockdown following a single administration of the Qiagen miR-145 ASO; therefore, we decided to perform a miR-145-5p level time course. Naïve mice were injected with the Qiagen control or miR-145 ASO at a dose of 20 µg/mouse and the mice were sacrificed at various timepoints following ASO treatment. Spleen, thymus and lumbar spinal cord tissue was dissected and relative level of miR-145-5p was analyzed by RT-qPCR. Again, there was no reduction in miR-145-5p in the lumbar spinal cord 24 h or 7 days following ASO treatment (Figure 8B). We did detect a significant reduction

in miR-145-5p in the spleen (Figure 8C) and a trend towards a reduction in miR-145-5p in the thymus (Figure 8D) 24 h, 7 days, 14 days and 21 days following treatment with the miR-145 ASO, demonstrating that a single dose of the miR-145 ASO was effective at knocking down miR-145-5p levels in lymphoid tissues for at least 21 days following administration. The miR-145 ASO was able to knockdown miR-145-5p in the periphery but not in the CNS, suggesting that the ASOs were unable to penetrate the CNS.

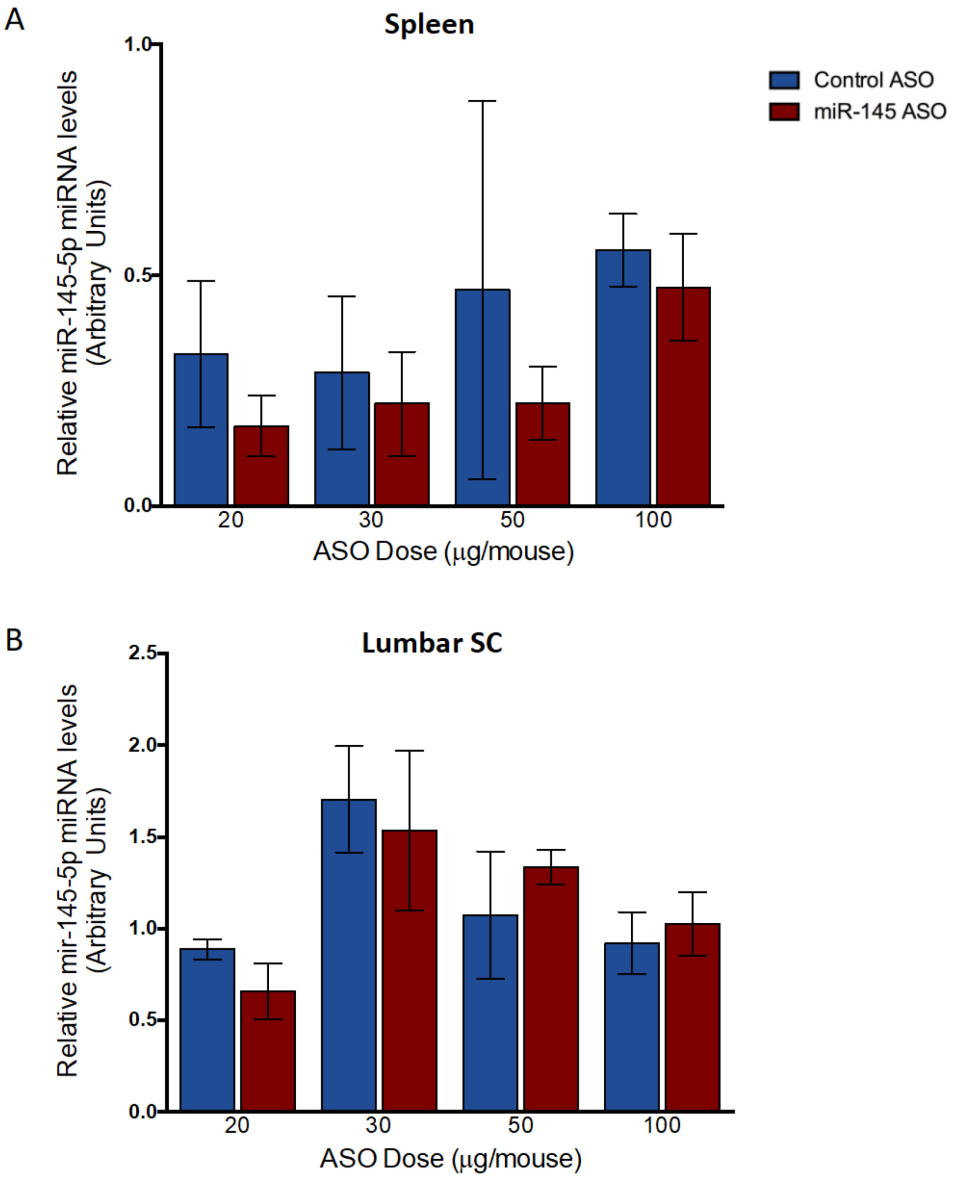

Figure 7. Fisher Scientific miR-145 ASO did not reduce miR-145 expression. Relative levels of miR-145-5p 24 h following treatment with the Fisher Scientific mirVana control and miR-145 ASOs at various doses in the spleen (A) and lumbar SC (B). Graphs show miR-145-5p miRNA levels relative to snU6. Values represent mean +/- SEM. Unpaired t test; n=3-4.

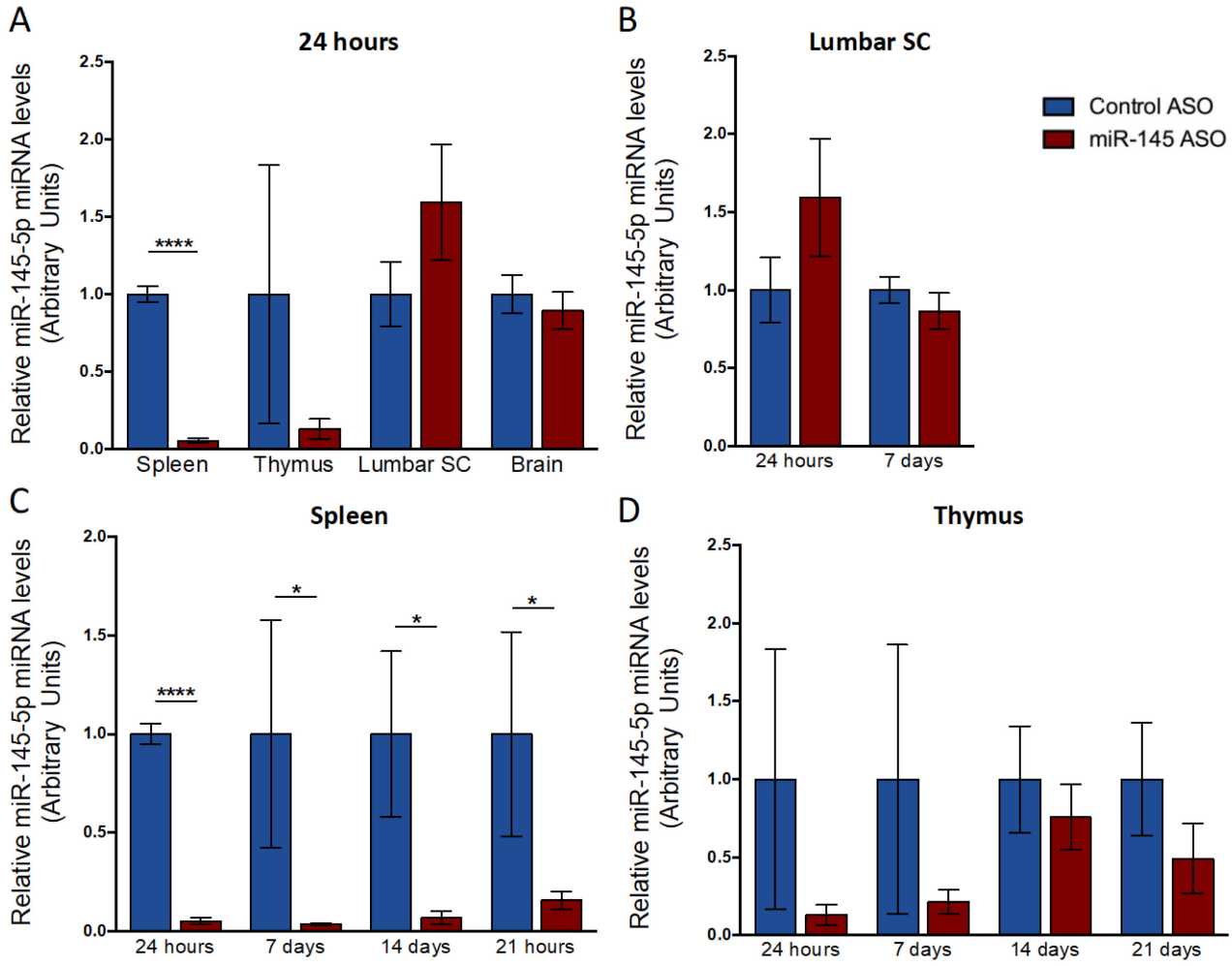

Figure 8. Qiagen miR-145 ASO reduced miR-145 in lymphoid tissue for up to 21 days following treatment. A. Relative level of miR-145-5p with the Qiagen custom *in vivo* miRCURY control and miR-145 ASOs in spleen, thymus, lumbar SC and brain tissue 24 h following treatment. B-D. miR-145-5p levels in lumbar SC (B), spleen (C) and thymus (D) at 24 h, 7 days, 14 days and 21 days following ASO administration. miR-145-5p miRNA levels relative to snU6 and normalized to control ASO. Values represent mean +/- SEM. Unpaired t-test; ∗=p<0.05, ****=p<0.0001; n=3-4.

3.2 miR-145 ASO reduced miR-145-5p in the CNS following EAE induction

Since EAE induction leads to disruption of the BSCB, we decided to investigate whether EAE induction would help the miR-145 ASO enter the CNS. EAE was induced in female mice, aged 10-13 weeks. The mice were injected with the Qiagen control or miR-145 ASO at the first incidence of disease. The mice were sacrificed 24 h following ASO treatment, and spleen, thymus and lumbar spinal cord tissue was dissected. Relative level of miR-145-5p was analyzed by RT-qPCR. There was a significant reduction in miR-145-5p levels in the spleen, thymus and lumbar spinal cord following administration of the miR-145 ASO (Figure 9). Relative level of miR-145-5p was reduced by ~75% in the spleen, ~97% in the thymus and ~42% in the lumbar spinal cord, demonstrating that miR-145-5p was knocked down in both periphery and CNS tissues. While the miR-145 ASO was only effective in the periphery of naïve mice, it was able to penetrate the CNS and knockdown miR-145-5p in the lumbar spinal following EAE induction.

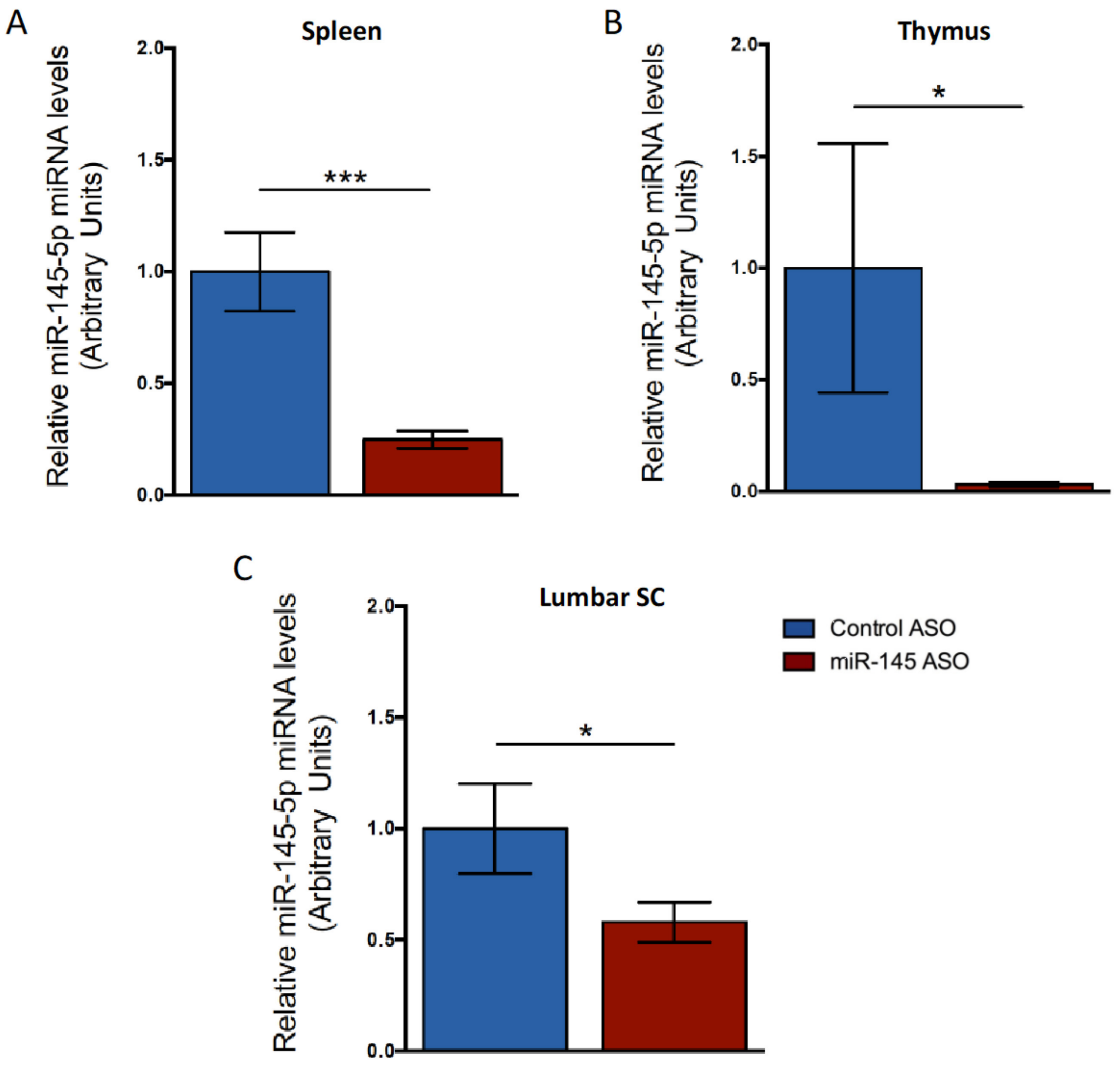

Figure 9. miR-145 is reduced in lymphoid and lumbar spinal cord tissue following miR-145 ASO administration at EAE onset. Relative level of miR-145-5p 24 h following administration of Qiagen custom *in vivo* miRCURY control and miR-145 ASOs at EAE onset in spleen (A), thymus (B) and lumbar SC (C). Graphs show miR-145-5p miRNA levels relative to snU6 and normalized to control ASO. Values represent mean +/- SEM. Unpaired t test; ∗=p<0.05, ***=p<0.001; n=3-4.

3.3 Clinical severity of EAE is improved with miR-145 ASO treatment

Following ASO optimization, we evaluated the effect of the miR-145 ASO at EAE onset on clinical severity of disease. Female mice, 10-13 weeks of age, were injected with the MOG_{35-55}/CFA emulsion and PTX on day 0 and PTX on day 1 (Figure 10A). The mice were not handled again until day 7 to allow EAE induction to occur. At the first incidence of disease (EAE score $>$ 0.0), the mice were injected with the control or miR-145 ASO at a dose of 20 µg/mouse. Mice were scored daily and weighed semi-daily from day 7 until day 30. The mice treated with the control ASO displayed normal trends for EAE score and weight loss throughout the course of the disease (Figure 10B,C). There was an exponential increase in EAE score following the onset of disease until the mice reached the peak of the disease, at which point the mice showed a slight reduction in EAE score (Figure 10B). The mice treated with the miR-145 ASO had a similar pattern in EAE score throughout the first half of the disease, but there is a reduction in EAE score during the chronic phases of the disease. The EAE score was significantly reduced from days 24 to 29. All of the mice showed a reduction in percent of starting weight following the onset of the disease that was consistent with the increased EAE score, but there were no significant differences between the treatment groups (Figure 10C). Overall, the miR-145 ASO improved the severity of disease in EAE mice.

When observing the time to disease onset, there were no differences between the two treatment groups (Figure 11A). As well, both groups had a mean onset day of ~12 and a mean EAE onset score of ~1.0 (Figure 11B,C). These consistencies were expected since the ASOs were not yet administered at this time. These results demonstrate that the two treatment groups were equivalent before ASO treatment.

The peak of the disease is defined as the day the mice first reach complete hind limb paralysis (EAE score $\geq$ 3.0). The time to hind limb paralysis was not different between the control or miR-145 ASO treatment groups (Figure 12A). As well, the days from first symptom of EAE to hind limb paralysis were ~2.5 for both groups (Figure 12B). The mean maximum clinical score is the highest score reached throughout the course of EAE. The mice treated with the control ASO had a mean maximum score of greater than 3.0 and the mice treated with the miR-145 ASO had a mean maximum score of less than 3.0; however, there was not a significant difference between the treatment groups (Figure 12C). Together, these results suggest that the miR-145 ASO does not significantly alter the peak of EAE.

The total number of days paralyzed was calculated in mice that reached complete hind limb paralysis. The mice treated with the control ASO were paralyzed for ~11 days and the mice treated with the miR-145 ASO were paralyzed for ~5 days; demonstrating that the length of paralysis is significantly reduced following miR-145 ASO administration (Figure 13A). Mice were monitored until day 30, which was arbitrarily set as the chronic timepoint. The mean score at the chronic phase of EAE was significantly reduced following treatment with the miR-145 ASO (Figure 13B). The mean score at day 30 was ~2.5 for the mice treated with the control ASO and ~2.0 for the mice treated with the miR-145 ASO.

The number of incidences of paralysis was also reduced in the mice treated with the miR-145 ASO (Figure 13C). The majority of the control ASO-treated mice experienced more than one instance of paralysis (66.67%) and the rest experienced just one instance of paralysis (33.33%). The percentage of the miR-145 ASO-treated mice that experienced more than one instance of paralysis was reduced (17.65%) and the percentage of mice that experienced just

one instance of paralysis was increased (65%). As well, some mice treated with the miR-145 ASO never reached complete hind limb paralysis (17.65%). These results demonstrate there is a reduction in the number of relapses with miR-145 ASO treatment.

Overall, the severity of EAE was decreased with administration of the miR-145 ASO. There were significant reductions in the EAE score during the later phase of EAE, the number of days paralyzed, the score at the chronic timepoint and number of relapses. Therefore, the miR-145 ASO improved the clinical severity of EAE.

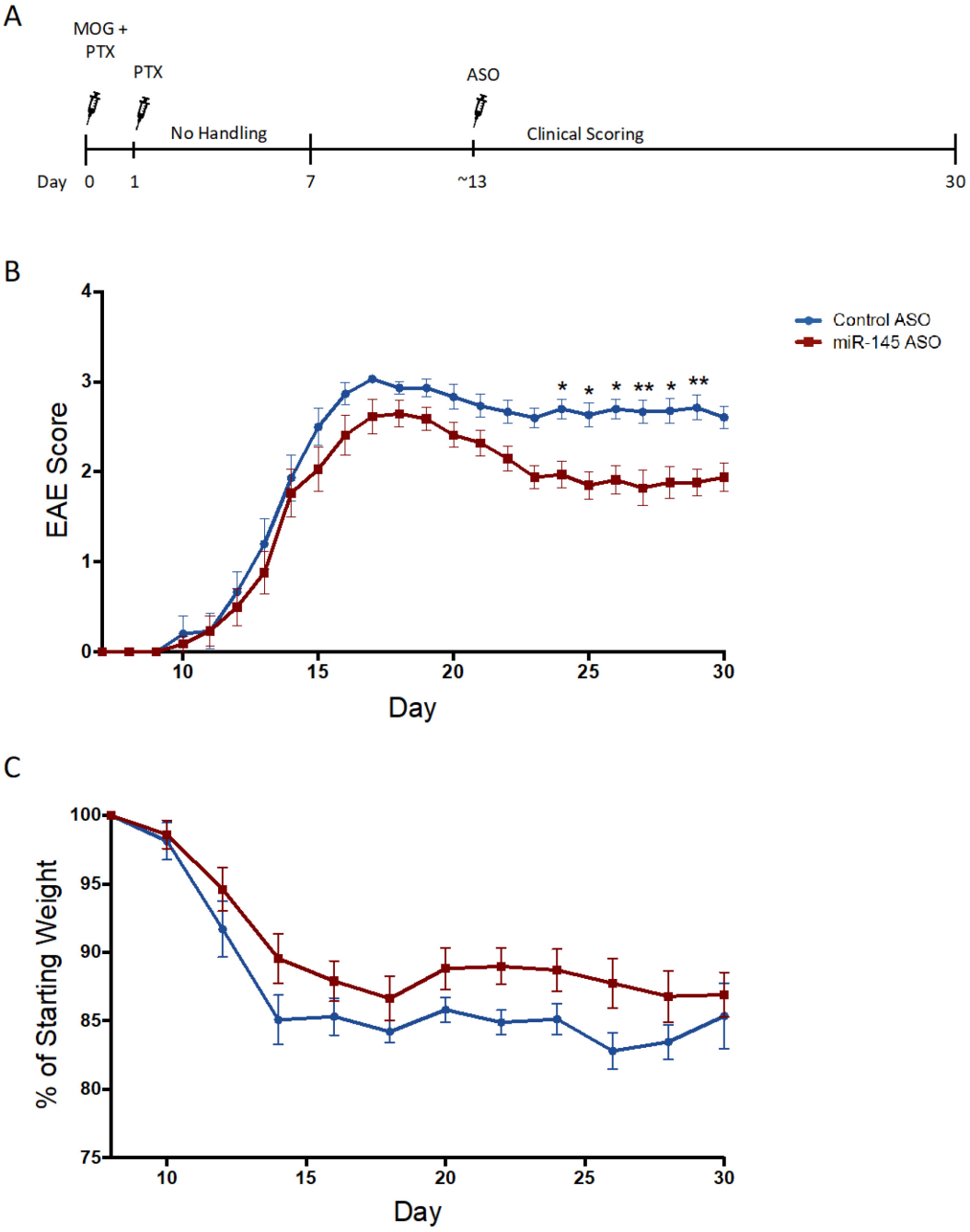

Figure 10. Clinical course of EAE is altered with miR-145 ASO treatment. A. Schematic of EAE induction, antisense oligonucleotide (ASO) treatment and clinical assessment. Mice are injected with myelin oligodendrocyte glycoprotein (MOG) antigen in complete Freund's adjuvant and pertussis toxin (PTX) on Day 0. The mice are given a second injection of PTX on Day 1. Mice were monitored daily from Days 7-30 and treated with the control or miR-145 ASO at EAE onset. B. Mean clinical scores during EAE time course. C. Mean weights expressed as percent of starting weight. B/C. Values represent mean +/- SEM. Two-way ANOVA with sidak post-hoc test; *=p<0.05, **=p<0.001; N=15-17.

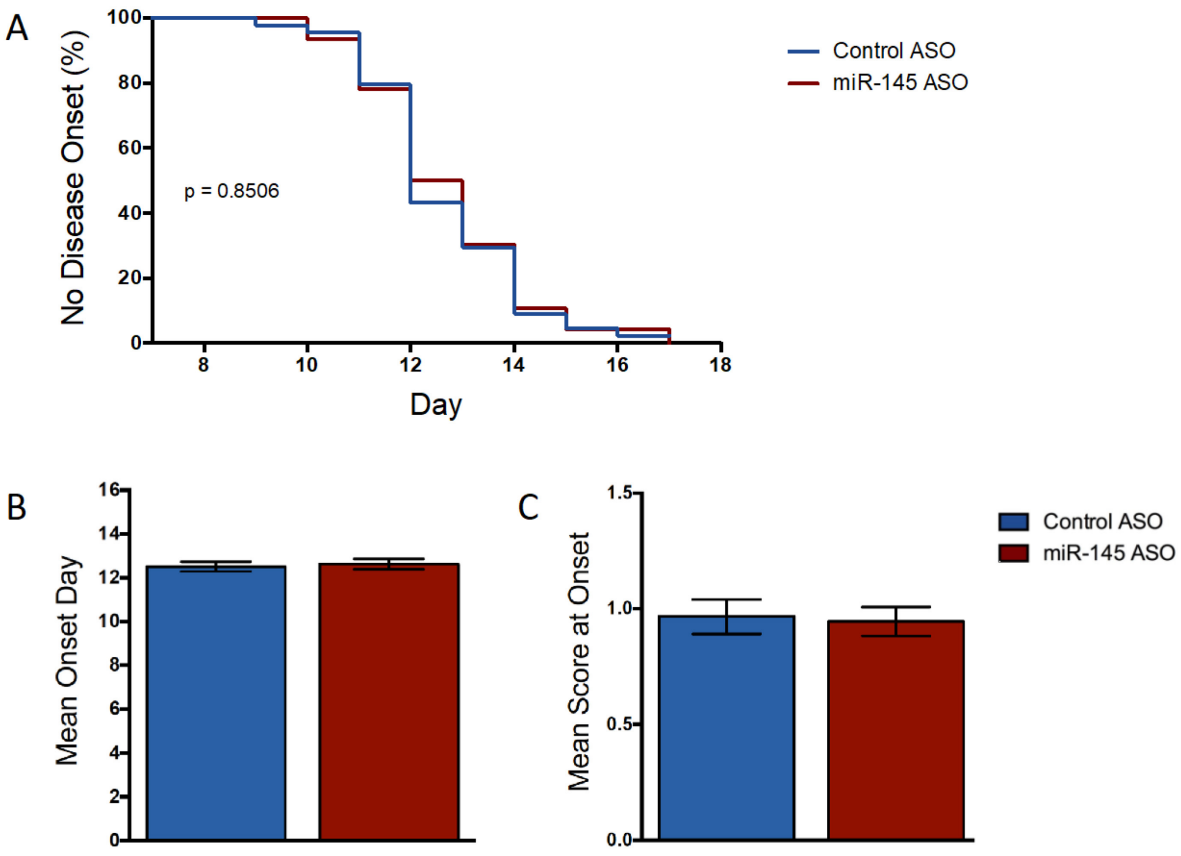

Figure 11. EAE onset is consistent between the two treatment groups before ASO administration. A. Kaplan Meier curve showing time to disease onset. Values represent percentage of mice who have not reached disease onset. Log-rank test; n=43-45. B. Mean onset day. C. Mean score at onset. B/C. Values represent mean +/- SEM. Unpaired t test; n=43-45.

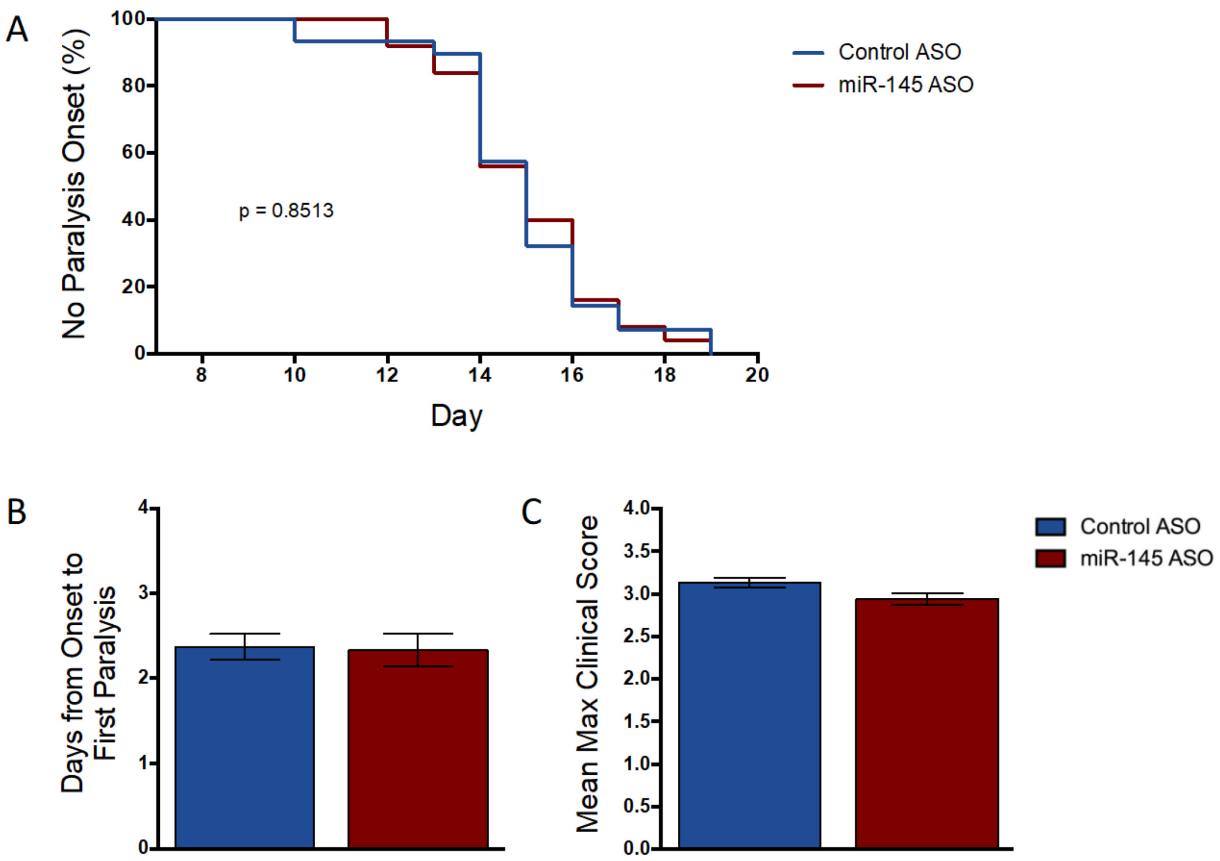

Figure 12. miR-145 ASO does not significantly alter the peak of EAE. A. Kaplan Meier curve showing time to paralysis onset. Values represent percentage of mice who have not reached paralysis onset. Log-rank test; n=24-27. B. Mean time from onset to paralysis, n=43-45. C. Mean maximum clinical score, n=15-17. B/C. Values represent mean +/- SEM. Unpaired t-test.

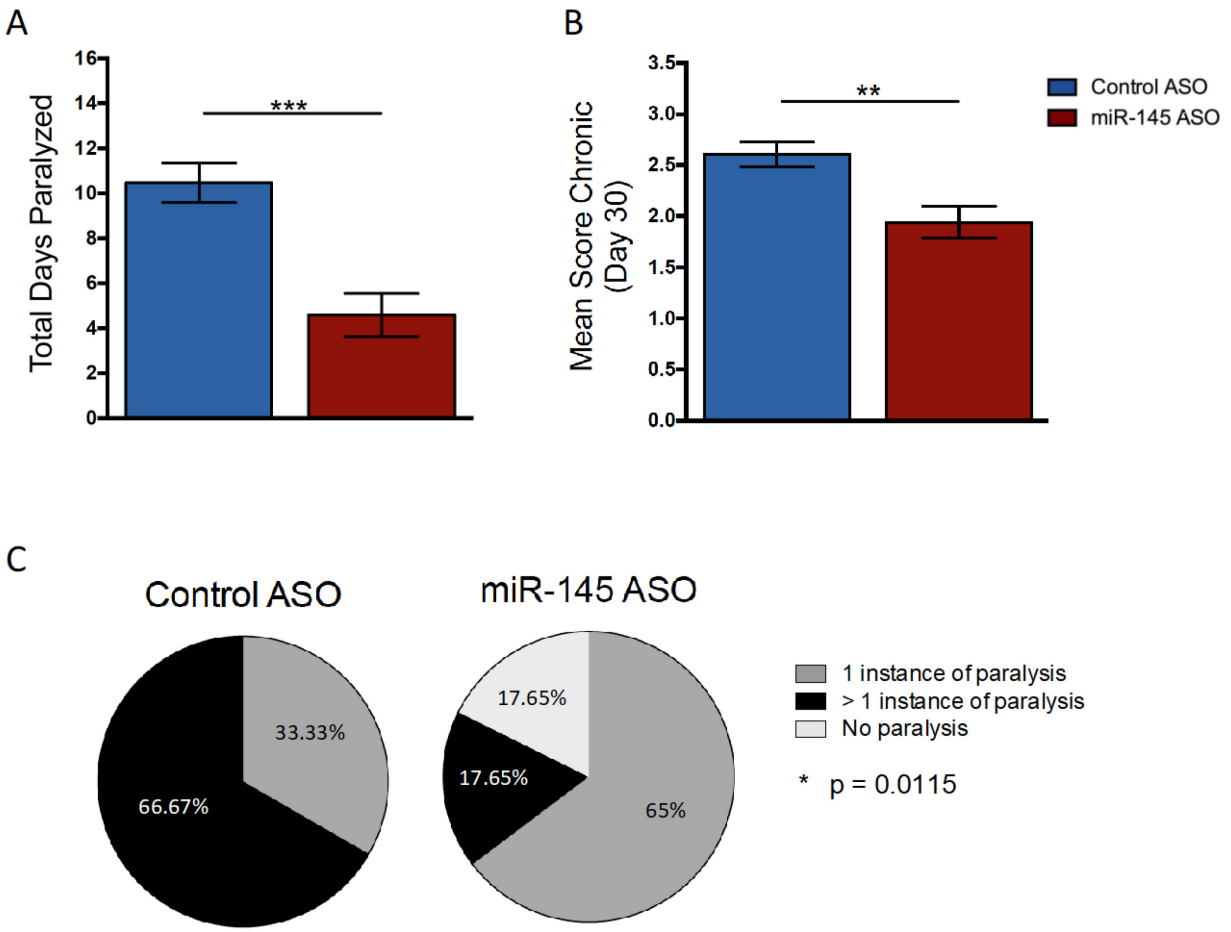

Figure 13. miR-145 ASO reduces the total days paralyzed, mean score at the chronic timepoint and number of relapses. A. Mean total days paralyzed. B. Mean score at chronic phase of EAE (Day 30). A/B. Values represent mean +/- SEM. Unpaired t-test. C. Proportions of all EAE-induced mice who exhibited no paralysis, 1 instance of paralysis or >1 instance of paralysis during the 30-day disease course. Values represent percentages. Chi-square test. A-C. **=p<0.001, ***=p<0.001; n=15-17.

3.4 Inflammation is decreased in the CNS but not the periphery of EAE mice following miR-145 ASO administration

Spleen and lumbar spinal cord tissues were collected to investigate the cellular and molecular changes associated with improvements in clinical severity of EAE following miR-145 ASO administration. Tissues were collected from naïve mice, and mice at the onset, peak and chronic phase of EAE. For all experiments, onset was 24 h following ASO treatment, peak was the first day that the mice reached a score of 3.0 or higher, and chronic was day 30. Tissues were processed for RT-qPCR, histology, immunohistochemistry and transmission electron microscopy.

As previously mentioned, EAE involves an inflammatory cascade that begins in the periphery and moves into the CNS. There are many factors associated with the inflammatory response following EAE induction, including changes in the expression of cytokines and chemokines. We decided to measure the gene expression of cytokines *IFNγ*, *Il1β*, *Il6* and *TNF*α, and chemokines *Ccl5* and *Cxcl1* because they have been shown to be involved in EAE development (Karpus, 2020). The expression of these cytokines and chemokines was measured in lymphoid and CNS tissue by RT-qPCR.

The mice treated with the control ASO showed some trends in the expression of *IFNγ*, *Il1β*, *Il6*, *Ccl5* and *Cxcl1* in the spleen of mice with EAE compared to naïve mice (Figure 14). There was a gradual reduction in *IFNγ* expression (Figure 14A) and a gradual increase in *Il6* expression (Figure 14C) over the course of EAE. *Il1β* was upregulated at onset and peak of disease (Figure 14B). *Ccl5* was downregulated (Figure 14E) and *Cxcl1* (Figure 14F) was upregulated at the onset and chronic phases of EAE. These expression profiles demonstrate that these cytokines and chemokines are involved in the peripheral immune response during

EAE. All of the cytokines and chemokines studied were greatly overexpressed in the lumbar spinal cord of mice with EAE compared to naïve mice (Figure 15). *IFNγ*, *Il1β*, *Il6*, *TNFα* and *Cxcl1* (Figure 15A-D,F) were all highest at onset, whereas *Ccl5* (Figure 15E) was highest during the peak and chronic phases of EAE. These expression profiles demonstrate that these cytokines and chemokines are important in the neuroinflammatory response following EAE induction.

In the spleen, there were no significant changes in the expression of *IFNγ*, *Il1β*, *Il6*, *TNFα, Ccl5* or *Cxcl1* (Figure 14). The mRNA levels of these cytokines and chemokines in the periphery are not associated with the improvements in clinical severity following miR-145 ASO administration. In the lumbar spinal cord, there were some alterations in the expression of cytokines and chemokines (Figure 15). Treatment with the miR-145 ASO resulted in a significant reduction in the expression of *Il1β* (Figure 15B) at onset, 24 h following ASO administration. It appeared as if there was upregulation of *IFNγ* (Figure 15A) at onset, downregulation of *Ccl5* (Figure 15E) at onset and upregulation of *Cxcl1* (Figure 15F) during the chronic phase; however, these differences were not significant. There were no differences in the expression of *Il6* and *TNFα* (Figure 15C,D) throughout the course of EAE. The few alterations in the expression of these cytokines and chemokines suggest that there may be a reduction in the neuroinflammatory response following miR-145 ASO administration.

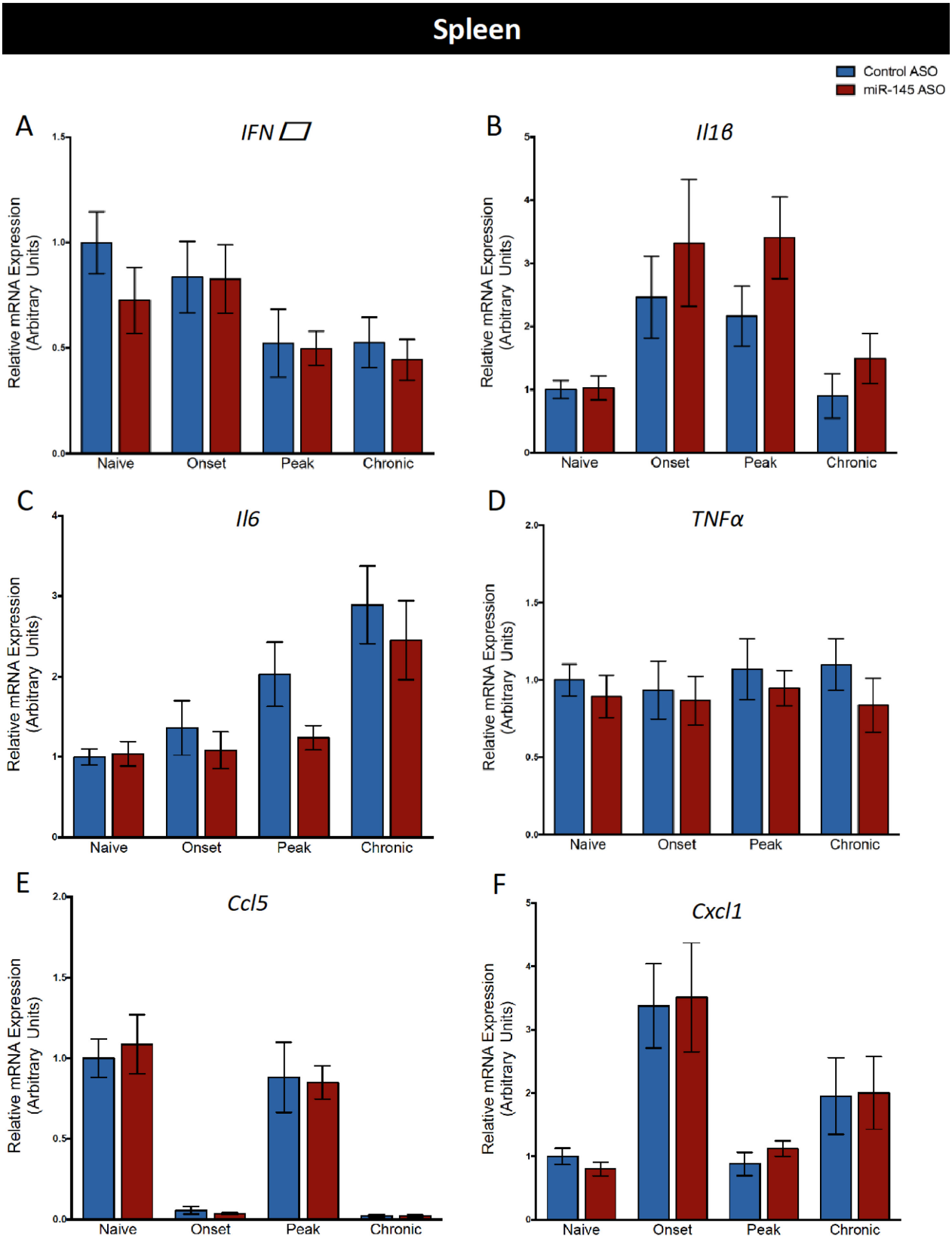
Spleen
Control ASO
miR-145 ASO
A
IFNγ
B
Il1β
C
Il6
D
TNFα
E
Ccl5
F
Cxcl1
Relative mRNA Expression (Arbitrary Units)
Naive
Onset
Peak
Chronic

Figure 14. Cytokine and chemokine expression is not significantly altered by miR-145 inhibition in the spleen over the course of EAE. Relative expression of cytokines *IFNγ*, *Il1β, Il6* and *TNFα*, and chemokines *Ccl5* and *Cxcl1* in the spleen in naïve mice and at onset, peak and chronic phases of EAE. Values represent mean +/- SEM. Two-way ANOVA with sidak post-hoc test. Normalized to *actb* and *ppia*; n=6-10.

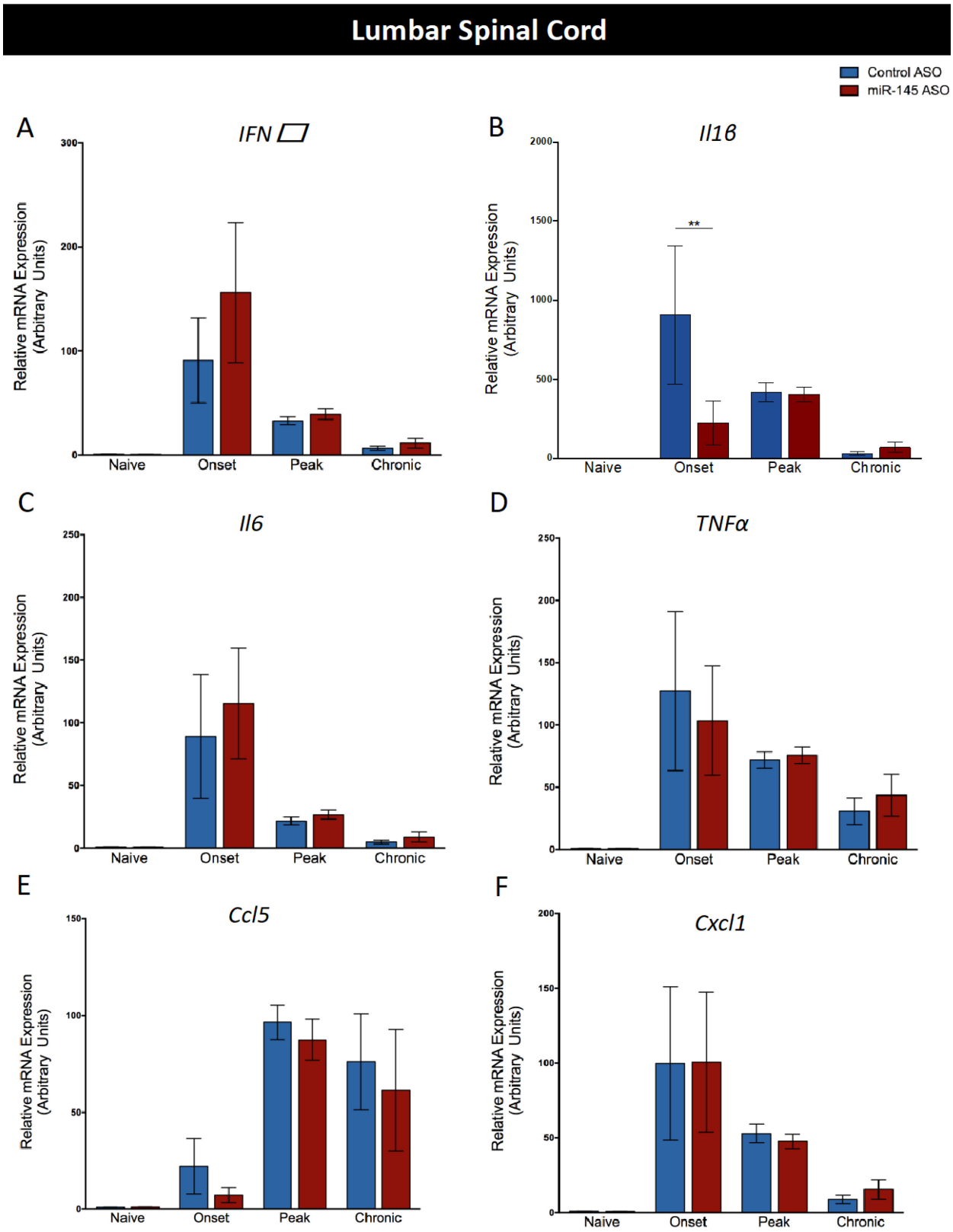
Lumbar Spinal Cord
Control ASO
miR-145 ASO
A
IFNβ
B
Il1β
C
Il6
D
TNFα
E
Ccl5
F
Cxcl1
Relative mRNA Expression (Arbitrary Units)
Naive
Onset
Peak
Chronic
**

Figure 15. There are few cytokine and chemokine expression alterations by miR-145 inhibition in the lumbar spinal cord over the course of EAE. Relative expression of cytokines *IFNγ*, *Il1β, Il6* and *TNFα*, and chemokines *Ccl5* and *Cxcl1* in the lumbar spinal cord in naïve mice and at onset, peak and chronic phases of EAE. Values represent mean +/- SEM. Two-way ANOVA with sidak post-hoc test. Normalized to *actb* and *ppia*. ∗∗=p<0.01; n=6-10.

We also wanted to evaluate if the miR-145 ASO would influence the neuroinflammatory response at the cellular level. Lumbar spinal cords were cross-sectioned and stained with hematoxylin and eosin (H&E) to measure immune cell infiltration. The hematoxylin stains cell nuclei purple and the eosin stains extracellular matrix and cytoplasm pink. Cellular infiltration is indicated by areas of dense nucleation, specifically in the submeningeal and parenchymal regions (Figure 16I). Percent infiltration area was calculated by measuring the nucleus-dense area relative to the total spinal cord area.

As expected, there was no cellular infiltration in the naïve mice treated with the control or miR-145 ASOs (Figure 16A,B). There were several areas of cellular infiltration in both treatment groups during EAE onset (Figure 16C,D). There was an increase in cellular infiltration during the peak of EAE (Figure 16E,F) in both treatment groups. There was extensive cellular infiltration in the control but not miR-145 ASO-treated mice during the chronic phase of EAE (Figure 16G,H). Quantification of the percent infiltration area demonstrates that the miR-145 ASO caused a slight reduction in the percent infiltration during the onset (Figure 16J) and peak (Figure 16K) phases of EAE; however, these changes are not statistically significant. There was a significant reduction in cellular infiltration in the miR-145 ASO-treated mice during the chronic phase of EAE. Cellular infiltration was reduced by ~60% during the chronic phase. The reduction in percent infiltration area demonstrates that the miR-145 decreases inflammation in the lumbar spinal cord, particularly during the chronic phase of EAE.

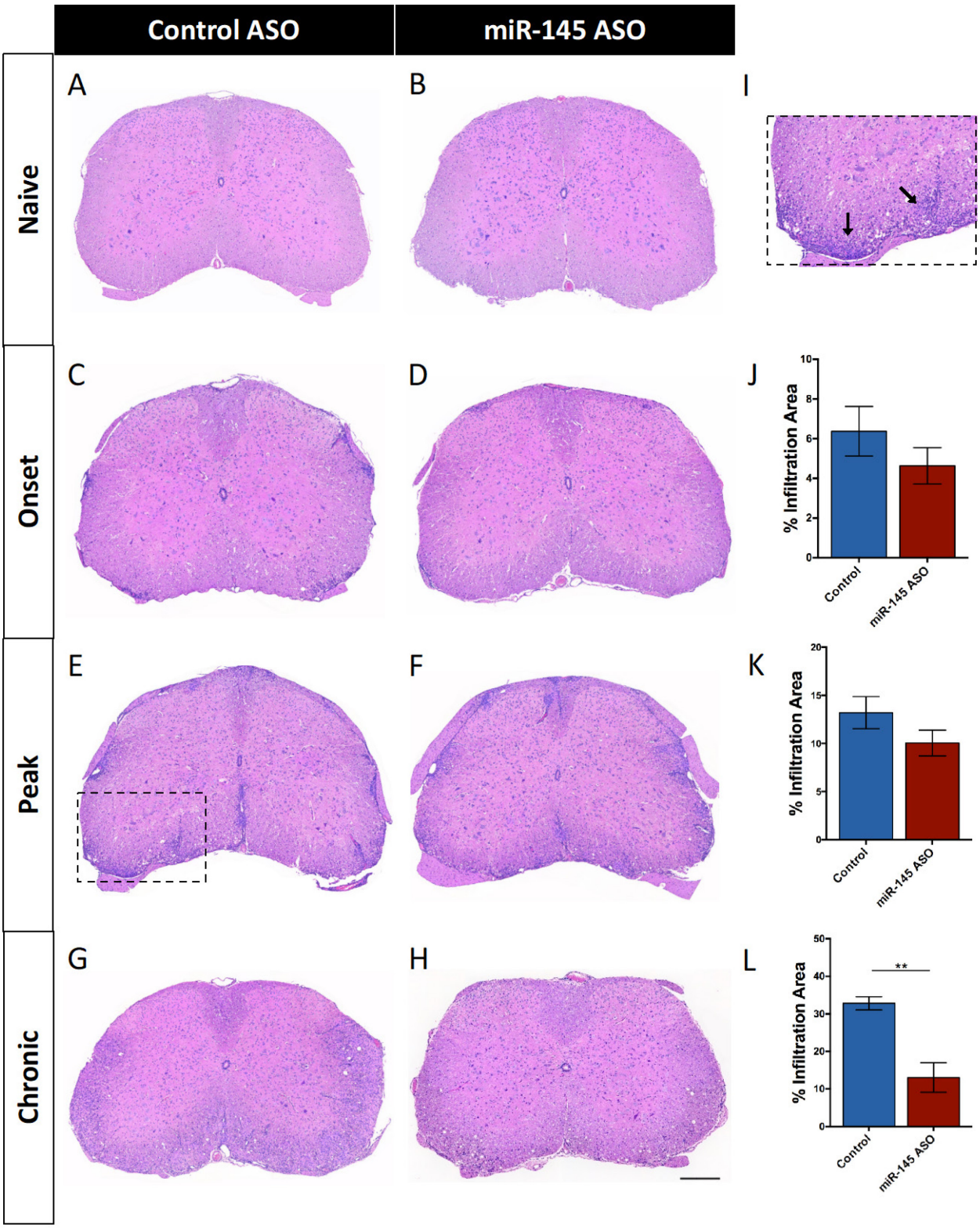
Control ASO
miR-145 ASO
Naive
Onset
Peak
Chronic
A
B
I
C
D
J
E
F
K
G
H
L
% Infiltration Area
Control
miR-145 ASO
**

Figure 16. Cellular infiltration of lumbar spinal cord is significantly reduced during the chronic phase of EAE with miR-145 inhibition. A-H. Hematoxylin and eosin stained lumbar spinal cord sections from naive (A/B) and onset (C/D), peak (E/F) and chronic (G/H) phases of EAE in mice treated with the control (left panel) and miR-145 (right panel) ASOs. Scale bar = 200 μm. I. Representative image of cellular infiltration in submeningeal and parenchymal regions (black arrows) from (E). J-L. Quantifications of percent infiltration area at onset (J), peak (K) and chronic (L). Values represent mean +/- SEM. Unpaired t-test; **=$p<0.001$; n=3-4.

3.5 Astrocyte and microglial activity are increased in the miR-145 ASO-treated mice during the chronic phase of EAE

Since there was a reduction in inflammation in the CNS during the chronic phase of EAE after miR-145 ASO treatment, we decided to assess the activation of CNS-resident immune cells. Astrocytes and microglia have been implicated in the neuroinflammatory response in EAE; therefore, we examined their activation following EAE induction. Mice were treated with the control or miR-145 ASO at the first incidence of disease and lumbar spinal cords were collected at the onset, peak and chronic phases of EAE. Naïve mice treated with the control or miR-145 ASO were used as controls. Lumbar spinal cords were cross-sectioned and immuno-stained for glial fibrillary acidic protein (GFAP) and ionized calcium-binding adapter molecule 1 (Iba1). GFAP is a marker for reactive astrocytes and Iba1 is a marker for reactive microglia (Ohsawa et al., 2004; Li et al., 2020). Total reactive astrocyte numbers were quantified by counting the number of $GFAP^+$ cells over the entire lumbar spinal cord section and total reactive microglia numbers were quantified by counting the number of $Iba1^+$ cells in the lumbar spinal cord parenchyma, excluding areas of dense nucleation.

When examining the GFAP-stained lumbar spinal cord sections of the control ASO-treated mice, the naïve mice had the lowest number of reactive astrocytes (Figure 17A). There was an increase in the number of astrocytes throughout EAE with the highest number of astrocytes during the chronic phase (Figure 17B-D). The miR-145 ASO treatment did not appear to affect the number of astrocytes in the naïve mice, or during the onset or peak phases of EAE, but there is a decrease in the number of astrocytes during the chronic phase (Figure 17E-H). Quantification of the mean number of reactive astrocytes per section demonstrates that there are no differences between the control or miR-145 ASO-treated mice in the naïve, onset or

peak mice (Figure 17I). There is a significant reduction in the number of astrocytes during the chronic phase of EAE. The number of astrocytes following miR-145 ASO administration is reduced by ~40% at the chronic phase of EAE. There are also fewer astrocytes during the chronic phase than the onset phase with miR-145 ASO treatment.

When examining the Iba1-stained lumbar spinal cord sections of the control ASO-treated mice, the naïve mice had the lowest number of reactive microglia (Figure 18A). The number of microglia increased during the onset and peak phases of EAE with the peak phase having the highest number of microglia (Figure 18B-C). The number of microglia is slightly lower during the chronic phase of EAE (Figure 18D). The miR-145 ASO treatment did not appear to affect the number of microglia in the naïve mice, or during the onset or peak phases of EAE (Figure 18E-G). There appeared to be a decrease in the number of astrocytes during the chronic phase of EAE (Figure 18H). Quantification of the mean number of reactive microglia in the parenchyma per section demonstrates that there are no differences during the naïve, onset or peak phases of EAE following miR-145 ASO treatment (Figure 18I). However, the number of microglia during the chronic phase of EAE is significantly reduced by ~30% following ASO administration. There was also a similar number of microglia during the chronic and onset phases with miR-145 ASO treatment

The reduction in astrocyte and microglia activation following miR-145 ASO treatment during the chronic phase of EAE is consistent with the reduction in cellular infiltration. Together, these results suggest that the miR-145 ASO reduces inflammation in the lumbar spinal cord. The decreased immune response may contribute to the clinical improvements seen in the later phase of EAE with miR-145 ASO administration.

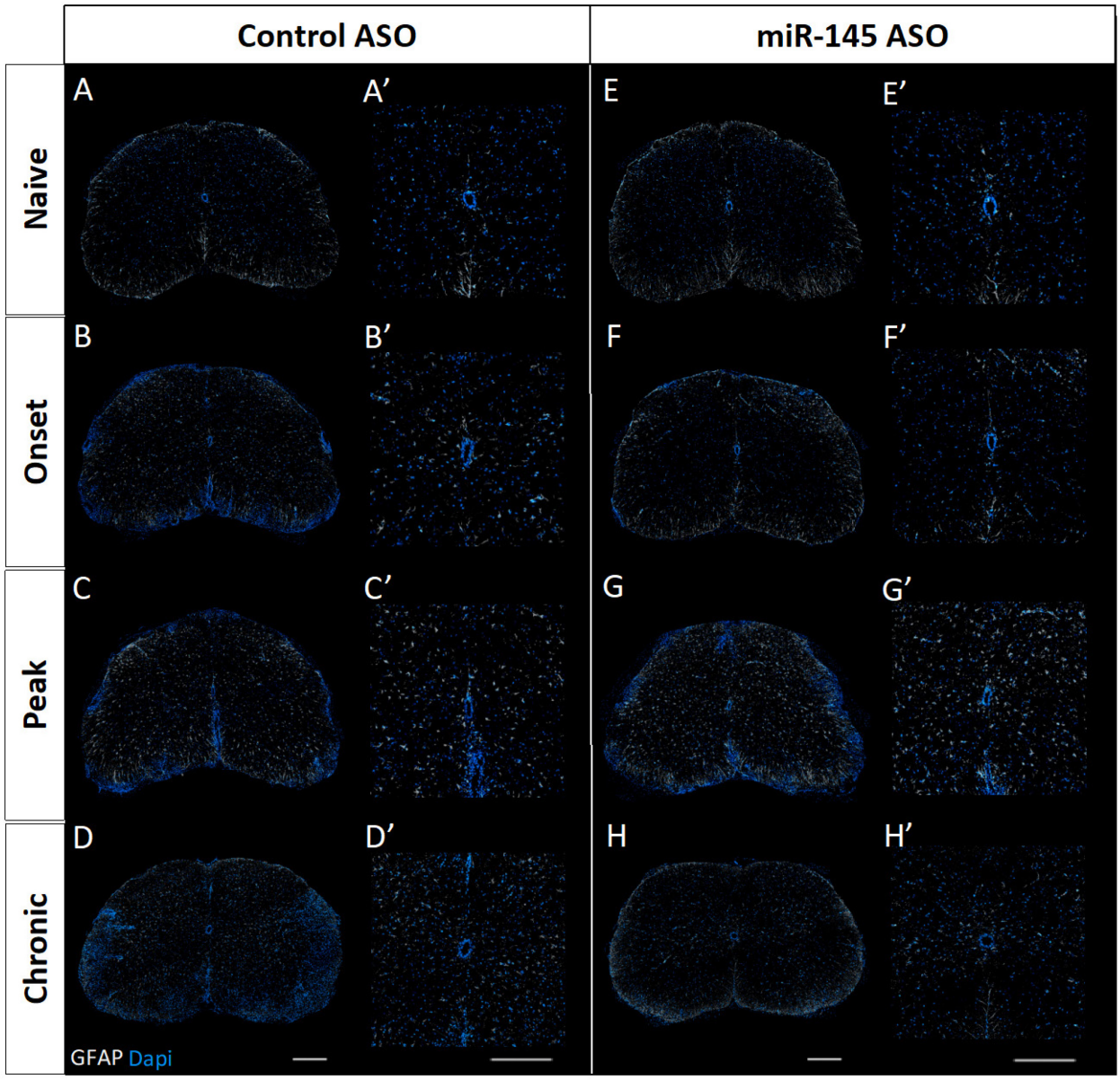
Control ASO
miR-145 ASO
Naive
Onset
Peak
Chronic
A
A'
E
E'
B
B'
F
F'
C
C'
G
G'
D
D'
H
H'
GFAP Dapi

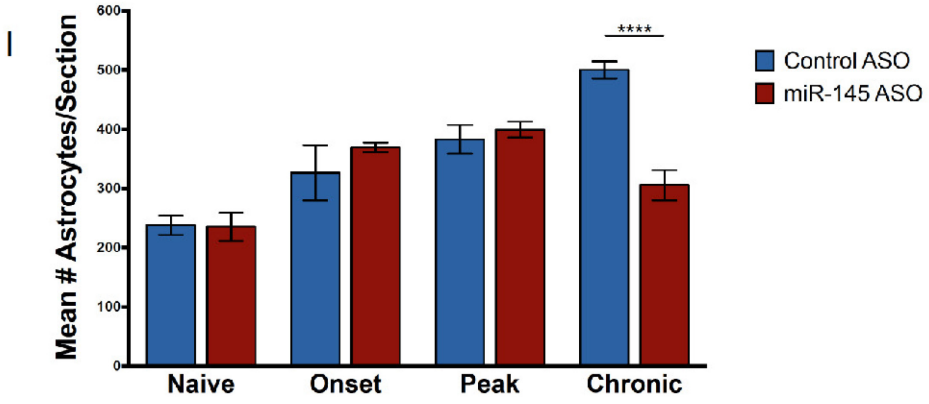
I
Mean # Astrocytes/Section
600
500
400
300
200
100
0
****
Control ASO
miR-145 ASO
Naive
Onset
Peak
Chronic

Figure 17. miR-145 ASO results in a decrease in the number of reactive astrocytes in the lumbar spinal cord during the chronic phase of EAE. A-H. Fluorescence micrographs of whole lumbar spinal cord from naive (A/B) and onset (C/D), peak (E/F) and chronic (G/H) phases of EAE in mice treated with the control (left panel) and miR-145 (right panel) ASOs. A'-H'. Magnified regions from A-H. Sections stained for GFAP (white) and counterstained with DAPI (blue). Scale bars = 200 μm. I. Quantification of number of $GFAP^+$ astrocytes per section. Values represent mean +/- SEM. Two-way ANOVA with Sidak post-hoc test; ****=$p<0.0001$; n=4.

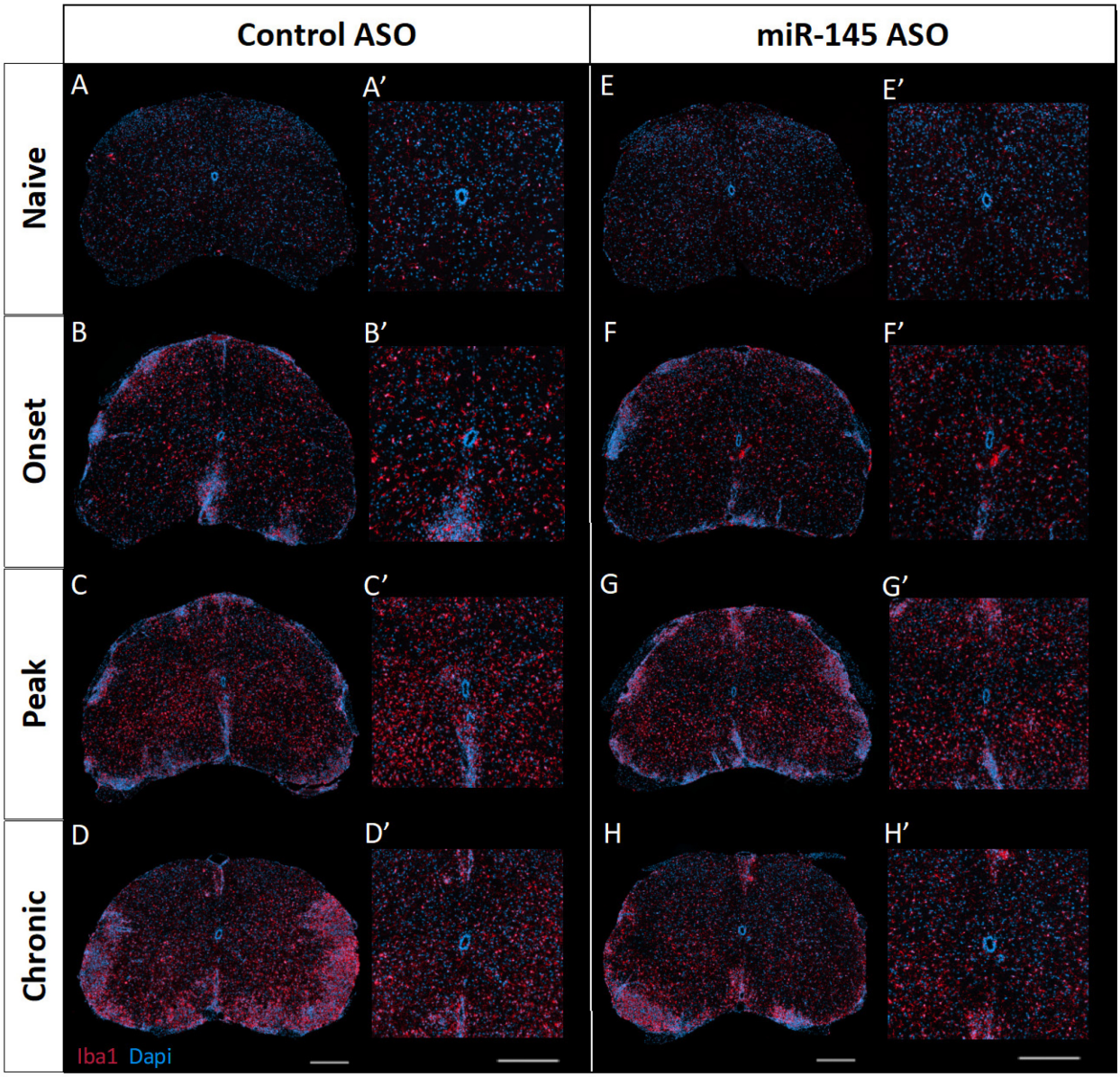
Control ASO
miR-145 ASO
Naive
Onset
Peak
Chronic
A
A'
B
B'
C
C'
D
D'
E
E'
F
F'
G
G'
H
H'
Iba1 Dapi

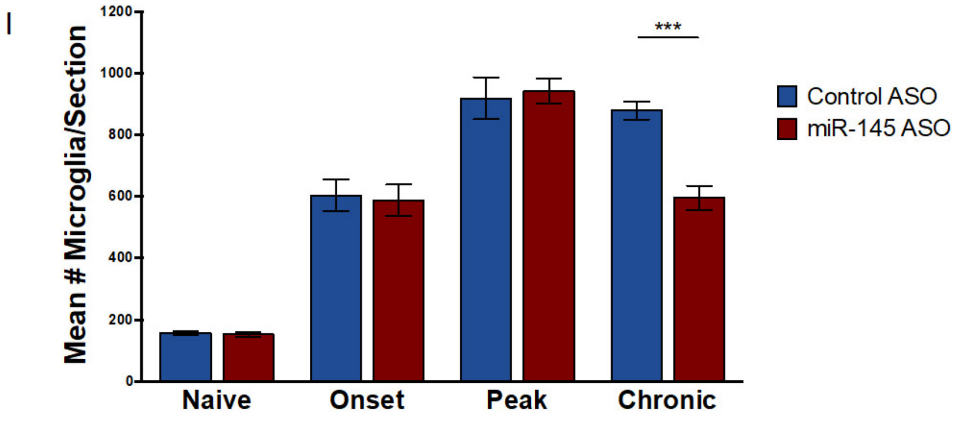
I
Mean # Microglia/Section
1200
1000
800
600
400
200
0
***
Control ASO
miR-145 ASO
Naive
Onset
Peak
Chronic

Figure 18. miR-145 ASO results in a decrease in the number of reactive microglia in the lumbar spinal cord during the chronic phase of EAE. A-H. Fluorescence micrographs of whole lumbar spinal cord from naive (A/B) and onset (C/D), peak (E/F) and chronic (G/H) phases of EAE in mice treated with the control (left panel) and miR-145 (right panel) ASOs. A'-H'. Magnified regions from A-H. Sections stained for Iba1 (red) and counterstained with DAPI (blue). Scale bars = 200 μm. I. Quantification of number of $Iba1^+$ microglia in the parenchyma per section. Values represent mean +/- SEM. Two-way ANOVA with Sidak post-hoc test; ***=$p<0.001$; n=4.

3.6 Myelination is improved in the spinal cord following miR-145 ASO treatment

EAE involves active immunization with myelin antigens, resulting in a myelin-specific immune response. This neuroinflammatory response results in damage to myelin and oligodendrocytes in the CNS. Since miR-145-5p has previously been shown to inhibit oligodendrocyte differentiation, we wanted to assess whether myelin retention was improved following treatment with the miR-145 ASO.

Mice were treated with the control or miR-145 ASO at the first incidence of disease and lumbar spinal cords were collected for RT-qPCR. We measured the expression of several myelin genes (*MAG*, *MBP* and *MOG*) in naïve mice, and at the onset, peak and chronic phases of EAE. *MAG* and *MBP* are expressed in developing and myelinating OLs, and *MOG* is only expressed in myelinating OLs (Han et al., 2013). All three genes encode for proteins found in myelin. MAG interacts with the axonal membrane to help myelin wrap around the axon. MBP is one of the most abundant proteins in myelin and is involved in myelin compaction. MOG is localized to the outer membrane of compacted myelin and functions as a cell adhesion molecule. These myelin proteins are all essential for myelin maintenance and function.

MAG and *MBP* but not *MOG* were slightly reduced at EAE onset (Figure 19A-C). Expression of *MAG*, *MBP* and *MOG* was lowest at the peak phase of EAE and then increased at the chronic phase of EAE, suggesting that there is demyelination and subsequent remyelination during EAE. There were no significant differences in the expression of *MAG*, *MBP* or *MOG* in the miR-145 ASO-treated mice compared to the control ASO-treated mice.

We also decided to measure expression of *MYRF* since it is a target of miR-145-5p (Kornfeld et al., 2021). There was a trend towards an increase in *MYRF* expression at onset in

the control ASO-treated mice compared to the miR-145 ASO-treated mice, but this change in expression was not significant (Figure 19D). *MYRF* was decreased during the peak and chronic phases of EAE compared to the naïve mice; however, there were no differences between the two treatment groups. Since MYRF is a target of miR-145-5p, we would expect to see increased *MYRF* expression following treatment with the miR-145 ASO. The expression of *MAG*, *MBP*, *MOG* and *MYRF* was not changed with miR-145 ASO treatment; however, protein expression could still be altered if they are regulated post-transcriptionally.

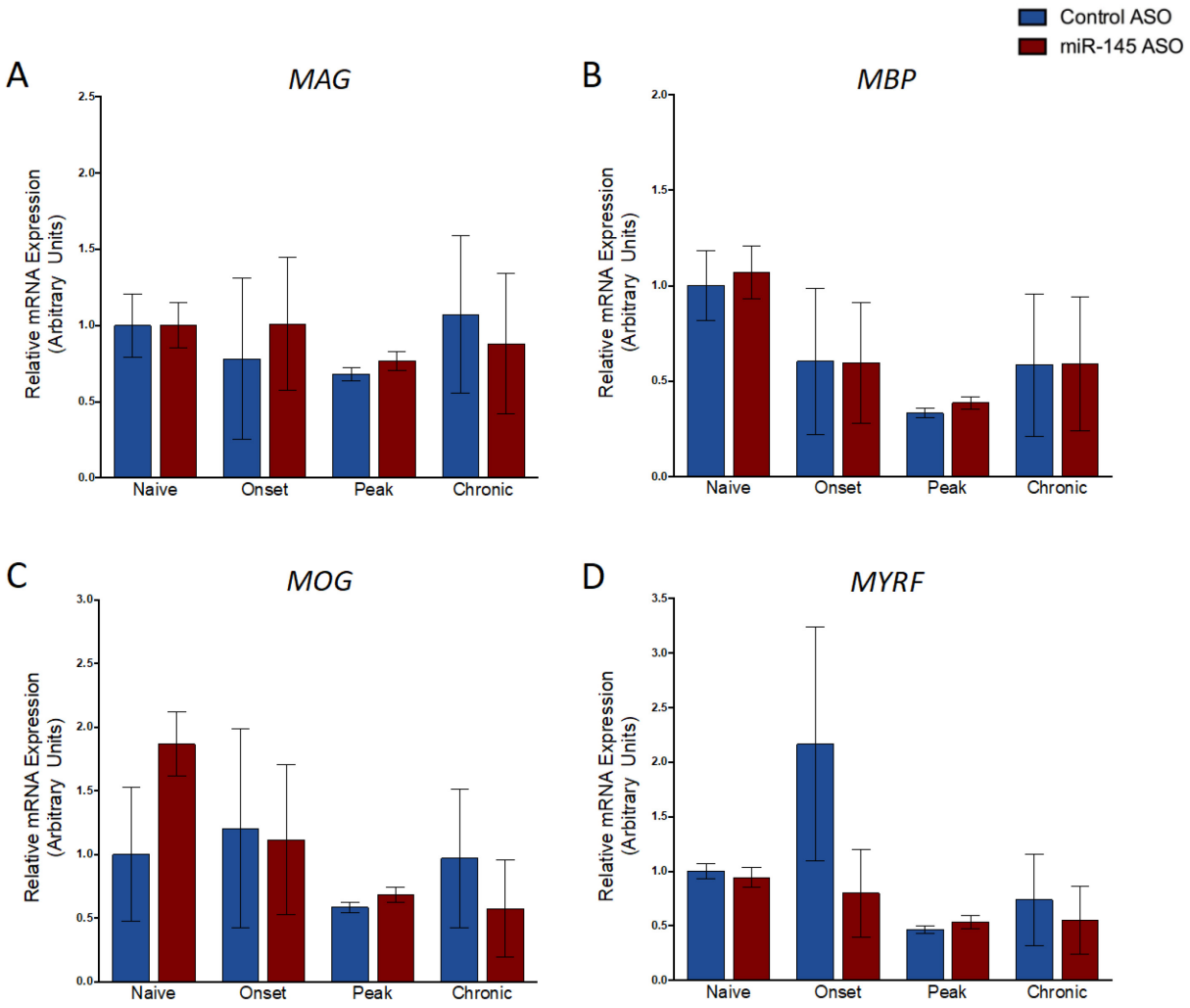

Figure 19. There are no significant differences in the expression of several myelin genes by miR-145 inhibition in the lumbar spinal cord over the course of EAE. Relative expression of *MAG* (A), *MBP* (B), *MOG* (C) and *MYRF* (D) in the lumbar spinal cord in naïve mice and at onset, peak and chronic phases of EAE. Values represent mean +/- SEM. Two-way ANOVA with sidak post-hoc test. Normalized to *actb* and *ppia*; n=6-8.

We wanted to further investigate whether myelin retention is affected by miR-145 ASO treatment; therefore, we decided to assess myelin content in the lumbar spinal cord with immunohistochemistry. Mice were treated with the control or miR-145 ASO and lumbar spinal cords were collected from naïve mice, and at onset, peak and chronic phases of EAE. Lumbar spinal cords were cross-sectioned and immuno-stained for MBP. As previously mentioned, MBP is one of the most abundant proteins in myelin; therefore, MBP staining is used to visualize myelination. Percent myelination area was calculated by measuring the MBP^+ area relative to the total spinal cord area.

As expected, the lumbar spinal cords from the naïve mice showed normal, thick myelination (Figure 20A,E). The control ASO-treated mice showed demyelination at the onset, peak and chronic phases of EAE (Figure 20B-D). The miR-145 ASO-treated mice also showed similar demyelination at onset and peak, but myelination appears to be slightly improved at the chronic phase of EAE (Figure 20F-H). When examining the corresponding MBP traces, the control ASO-treated mice showed a progressive decline in myelin area throughout EAE compared to the naïve mice (Figure 20A'-D'). The miR-145 ASO-treated mice also showed a progressive decline in myelin area from onset to peak compared to the naïve mice, but the myelin area appears to be increased during the chronic phase of EAE (Figure 20E'-H').

Quantification of the percent myelination area demonstrates that myelin area progressively decreases in the lumbar spinal cord throughout EAE (Figure 20I). While there appeared to be an increase in myelination area with the miR-145 ASO during the chronic phase, there were no significant differences in the percent myelination area with the miR-145 ASO compared to the control ASO at any timepoint. There is a significant reduction in percent

myelination area at the peak and chronic phases of EAE in the control ASO-treated mice compared to the naïve mice. The reduction in percent myelination area at the peak and chronic phases of EAE in the miR-145 ASO-treated mice compared to the naïve mice was not significant, suggesting that the miR-145 ASO may have a protective effect against demyelination and improve myelin retention.

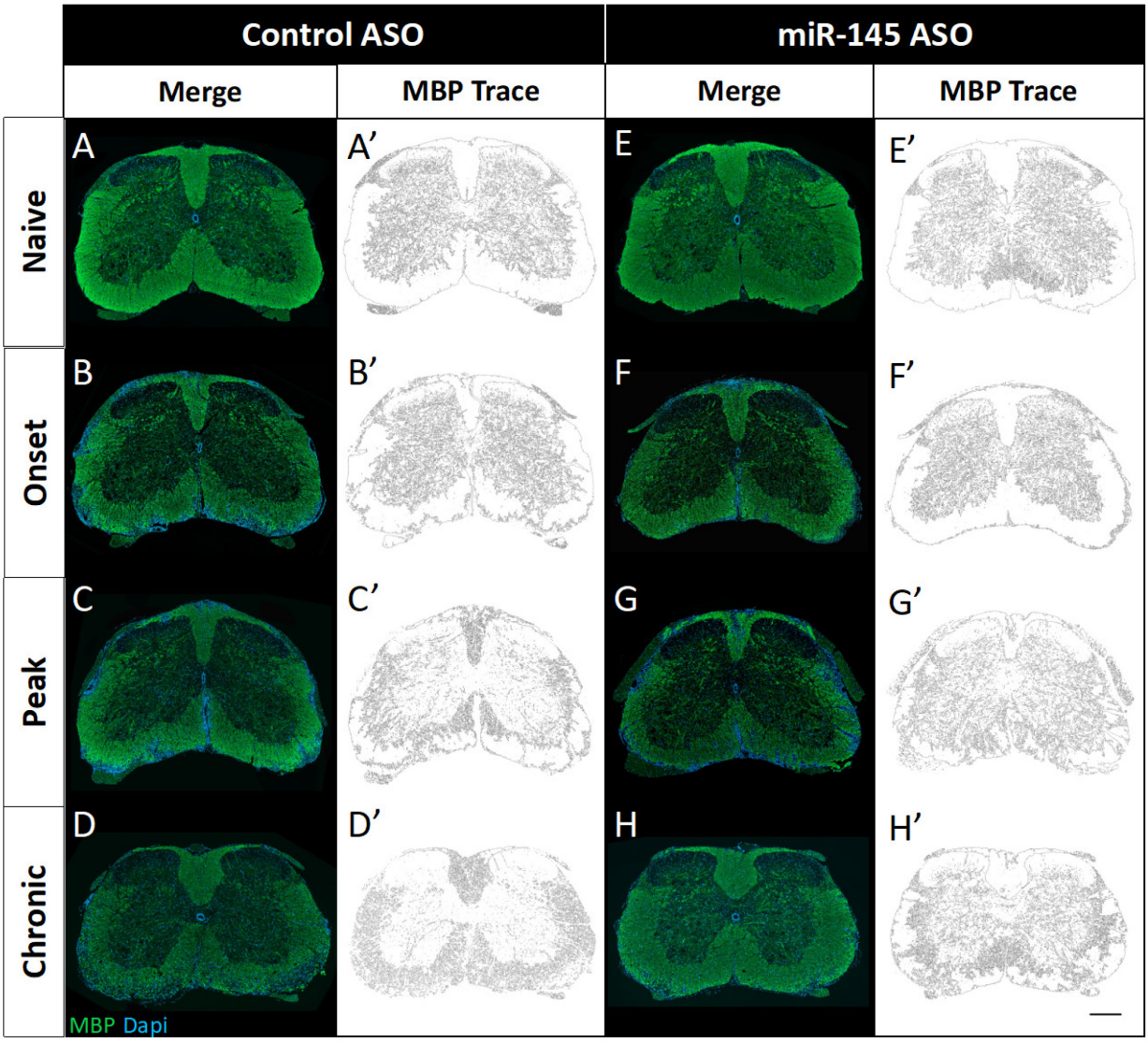
Control ASO
miR-145 ASO
Merge
MBP Trace
Merge
MBP Trace
Naive
Onset
Peak
Chronic
A
A'
E
E'
B
B'
F
F'
C
C'
G
G'
D
D'
H
H'
MBP Dapi

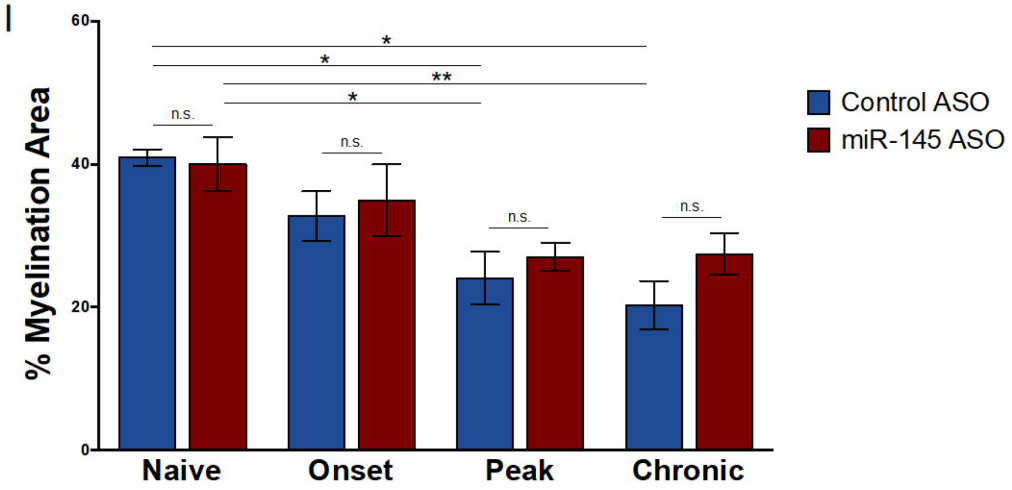
I
% Myelination Area
60
40
20
0
*
*
**
*
n.s.
n.s.
n.s.
n.s.
Naive
Onset
Peak
Chronic
Control ASO
miR-145 ASO

Figure 20. miR-145 ASO does not significantly increase myelination area in the lumbar spinal cord throughout EAE. A-H. Fluorescence micrographs of whole lumbar spinal cord from naive (A/B) and onset (C/D), peak (E/F) and chronic (G/H) phases of EAE in mice treated with the control (left panel) and miR-145 (right panel) ASOs stained for MBP (green) and counterstained with DAPI (blue). Scale bar=200 μm. A'-H'. MBP traces of of whole lumbar spinal cord from A-H. I. Quantification of percent myelination area. Values represent mean +/- SEM. Two-way ANOVA with Tukey post-hoc test; $*=p\leq0.05$, **=p<0.001; n=3-4.

Finally, we used transmission electron microscopy (TEM) to further investigate the effect of miR-145 ASO treatment on myelination in the lumbar spinal cord. Mice were treated with the control or miR-145 ASO and lumbar spinal cords were collected from naïve mice, and at onset, peak and chronic phases of EAE. Ultrathin lumbar spinal cord cross-sections were imaged with a TEM to observe the number of myelinated axons and myelin thickness. There are many thickly myelinated axons in the naïve mice treated with the control and miR-145 ASOs (Figure 21A). There appears to be a slight decrease in the number of myelinated axons and myelin thickness at onset with both ASOs. The control ASO-treated mice show extensive demyelination during the peak and chronic phases of EAE, as seen with a reduction in the number of myelinated axons, decreased myelin thickness and the presence of myelin debris surrounding the axons. The miR-145 ASO appears to improve myelination during the peak and chronic phases of EAE, with an increase in the number of myelinated axons and increased myelin thickness. Quantification of the number of myelinated axons per 100μm^2 demonstrates that there is a significant increase in the number of myelinated axons with the miR-145 ASO during the peak and chronic timepoints.

The increased number of myelinated axons in the lumbar spinal cord during the peak and chronic phases of EAE suggest that the miR-145 ASO improves myelin retention and/or remyelination in the later stages of EAE. The improvements in myelination likely contribute to the clinical improvements seen in the later phase of EAE following treatment with the miR-145 ASO.

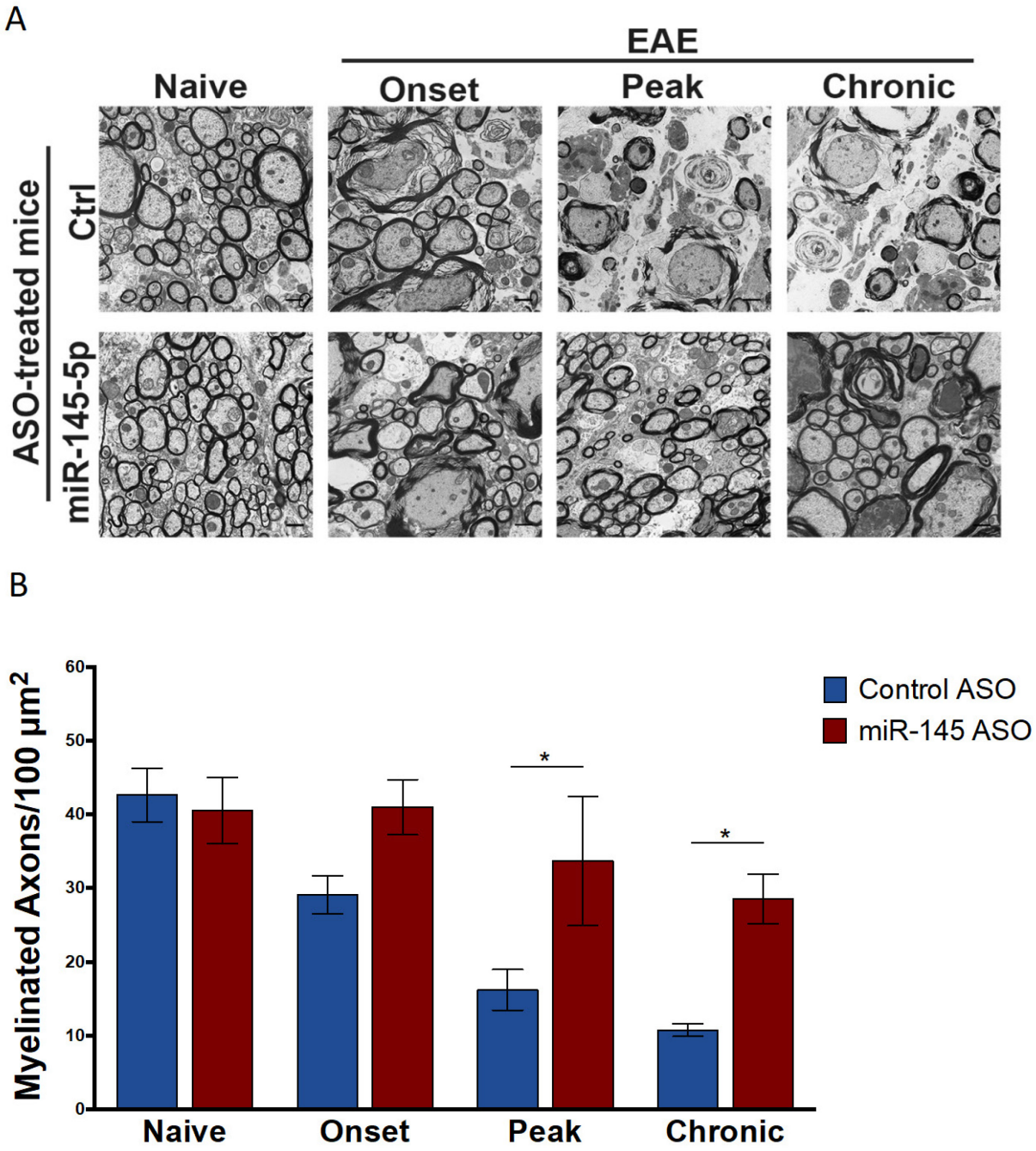

Figure 21. Neurons in the lumbar spinal cord have a greater number of myelinated axons following miR-145 ASO treatment. A. Representative transmission Electron Microscopy (TEM) micrographs of lumbar spinal cord sections from naïve mice and at onset, peak and chronic phases of EAE in mice treated with the control and miR-145 ASOs. Magnification of 10,000X. B. Quantification of myelinated axons per 100 um2. Values represent mean +/- SEM. Two-way ANOVA with Tukey post-hoc test; ∗=p≤0.05; n=3.

4. Discussion

MicroRNAs are important regulators of genes involved in both inflammation and myelination, and their dysregulation is seen in people with MS (de Faria Jr et al., 2012; Li and Yao, 2012; Jeker and Bluestone, 2013). A specific miRNA, miR-145-5p, plays a critical role in oligodendrocyte differentiation and it is upregulated in MS lesions (Keller et al., 2009; Letzen et al., 2010; Tripathi et al., 2019; Kornfeld et al., 2021). Our lab has shown that miR-145-5p KO mice exhibit improved remyelination in the chronic cuprizone model (Kornfeld *et al*., unpublished). miR-145-5p KO also resulted in reduced clinical severity, improved myelination and reduced inflammation in the EAE mouse model (Kornfeld *et al*., unpublished). We decided to investigate whether treatment with a miR-145 ASO at the onset of symptoms would also decrease the severity of the disease to examine the therapeutic potential of miR-145-5p inhibition.

4.1 ASO can knockdown miR-145-5p in the CNS following disruption of the BSCB

We decided to use an ASO to inhibit miR-145-5p in the EAE mouse model. As previously mentioned, ASOs are synthetic oligonucleotides that are designed to bind and inhibit specific RNAs (Rinaldi and Wood, 2017). The miR-145 ASOs used in this study were designed to specifically bind to and inhibit miR-145-5p. The control ASOs were designed such that they would not bind to any sequence in the mouse genome. We intravenously injected the mice with the control or miR-145 ASOs to observe the effects of miR-145-5p inhibition in both the periphery and the CNS. Two ASOs were tested but only the Qiagen miR-145 ASO successfully

reduced miR-145-5p in the spleen and thymus but not the lumbar spinal cord, suggesting that the ASO was unable to penetrate the BSCB and enter the CNS (Figures 7-8).

Integrity of the BSCB is impaired following EAE induction, allowing the entrance of peripheral immune cells into the CNS (Bennett et al., 2010; Constantinescu et al., 2011). Intravenous injection of the miR-145 ASO at the first incidence of EAE resulted in a significant reduction in the expression of miR-145-5p in the spleen, thymus and lumbar spinal cord (Figure 9). The ASO was only able to enter the CNS and target miR-145-5p when the BSCB was weakened. These results demonstrate that the ASO can be used to inhibit miR-145-5p in mouse models where the integrity of the BSCB or BBB are impaired, such as EAE. Another mechanism to allow the entrance of the miR-145 ASO into the CNS would be needed in mouse models without disruption of the BSCB or BBB.

4.2 Symptoms of EAE are improved with miR-145 ASO

Treatment with the miR-145 ASO resulted in improved clinical outcomes for the EAE-induced mice. The EAE score was significantly reduced throughout the later phase of EAE following treatment with the miR-145 ASO (Figure 10). The control and miR-145 treatment groups responded similarly to EAE prior to injection with the ASOs (Figure 11). There were no differences in the time from induction to disease onset, mean day of onset or mean score at onset. The mice were injected with the ASOs at onset of symptoms and there were improvements in clinical severity following treatment with the miR-145 ASO. While there were no significant differences in the peak of the disease, there was a trend towards a reduction in the mean maximum clinical score (Figure 12). The mice treated with the miR-145 ASO showed

significant improvements following the peak of the disease (Figure 13). There was a reduction in the total number of days paralyzed and a reduction in the EAE score at the chronic timepoint. The mice regained hind limb function faster and showed milder symptoms during the later phase of the disease. As well, there was a reduction in the number of relapses and some mice did not even reach complete hind limb paralysis. These results demonstrate that the miR-145 ASO resulted in improved recovery following the peak of the disease. Inhibition of miR-145-5p at EAE onset improved the clinical severity of EAE, suggesting that miR-145-5p has a critical role in the progression of EAE.

4.3 miR-145 ASO reduces inflammation and increases myelination during EAE

EAE involves a myelin-specific immune response that starts in the periphery and moves into the CNS (Robinson et al., 2014). Cytokines *IFNγ*, *Il1β*, *Il6 and TNFα*, and chemokines *Ccl5* and *Cxcl1* are dysregulated in EAE (Karpus, 2020). The expression of these cytokines and chemokines in the spleen was not significantly altered with the miR-145 ASO at any timepoint during EAE (Figure 14). The lack of changes to cytokine and chemokine expression in the spleen does not necessarily mean that the peripheral immune response is unchanged with miR-145 ASO treatment. In the lumbar spinal cord, there was a significant reduction in the expression of *Il1β* at EAE onset with miR-145 ASO treatment (Figure 15). Il1β is a pro-inflammatory cytokine that has been shown to be essential for the myelin-specific T cell response and subsequent neuroinflammation in EAE (Matsuki et al., 2006; Sutton et al., 2009; Hauptmann et al., 2020). There were also trends towards upregulation of *IFNγ* and downregulation of *Ccl5* at EAE onset, and upregulation of *Cxcl1* during the chronic phase. IFNγ KO has been shown to result in

increased neuroinflammation, whereas treatment with IFNγ results in improved clinical symptoms of EAE (Stoolman et al., 2018; Zhou et al., 2020). Ccl5 is a pro-inflammatory chemokine that recruits leukocytes to the site of inflammation and the knockout of its receptor has been shown to result in reduced immune infiltration into the CNS in EAE (Dos Santos et al., 2005; Gu et al., 2016). *Cxcl1* is a chemokine that is secreted by astrocytes and recruits OPCs (Vora et al., 2012; Watson et al., 2020). The changes in the gene expression of *Il1β, IFNγ, Ccl5* and *Cxcl1* in the lumbar spinal cord suggest that there is a reduction in the neuroinflammatory response with the miR-145 ASO.

The neuroinflammatory response was also altered at the cellular level with inhibition of miR-145-5p at the first incidence of the disease. There was a significant reduction in cellular infiltration into the lumbar spinal cord at the chronic phase of EAE following treatment with the miR-145 ASO (Figure 16). Following EAE induction, immune cells infiltrate and accumulate in the lumbar spinal cord. These infiltrates include leukocytes, neutrophils, dendritic cells and macrophages (Al-Shamsi et al., 2015; Wang et al., 2016; Brandão et al., 2020; Zhang et al., 2020). CNS-resident cells (astrocytes, microglia) also accumulate in the spinal cord and activate an immune response following EAE induction (Chu et al., 2018; Brambilla, 2019). We demonstrated that there was a significant reduction in astrocyte activation in the chronic phase of EAE with miR-145 ASO treatment (Figure 17). Reactive astrocytes have been shown to contribute to neuroinflammation during EAE through activation of microglia, production of cytokines and chemokines, and disruption of the BSCB (Brambilla, 2019). Interestingly, astrocyte-specific inhibition of nuclear factor kappa-light-chain enhancer of activated B cells (NFκB) results in decreased severity of EAE (Brambilla et al., 2009). NFκB is a transcription factor

that induces inflammation (Lawrence, 2009). miR-145-5p enhances NFκB activation resulting in increased expression of multiple pro-inflammatory cytokines, including Il1β, Il6 and TNFα (Wang et al., 2019). Therefore, inhibition of miR-145-5p could lead to downregulation of NFκB in astrocytes and a reduction in the production of pro-inflammatory cytokines. This pathway may explain the reduction in astrocyte activation in the chronic phase of EAE with miR-145 ASO treatment. We demonstrated that there was a significant reduction in astrocyte activation in the chronic phase of EAE with miR-145 ASO treatment (Figure 18). There are two known targets of miR-145-5p in microglia: Twist related protein 2 (Twist2) and nuclear receptor related 1 (Nurr1) (Su et al., 2014; Xie et al., 2017). Downregulation of Twist2 and Nurr1 by miR-145-5p results in downregulation of c-Maf and upregulation of TNFα, respectively. c-Maf is an anti-inflammatory transcription factor and TNFα is a pro-inflammatory cytokine. Therefore, inhibition of miR-145-5p could lead to upregulation of Twist2 or Nurr1 in the microglia, which would result in reduced neuroinflammation. One of these pathways could explain the reduction in microglial activation in the chronic phase of EAE with miR-145 ASO treatment. Together, the changes to cellular infiltration, astrocyte activation and microglial activation suggest that neuroinflammation is reduced during the chronic phase of EAE following treatment with the miR-145 ASO.

Inflammation in the CNS leads to demyelination following EAE induction (Patel and Balabanov, 2012). The expression of the myelin genes *MAG*, *MBP* and *MOG* was unaltered in the lumbar spinal cord with the miR-145 ASO at any timepoint during EAE (Figure 19). While the mRNA expression was unchanged, the protein expression could be affected if these genes are regulated post-transcriptionally. When observing MBP expression with immunohistochemistry,

we observed a trend towards an increase in percent myelination area at the peak and chronic timepoints with miR-145 ASO treatment (Figure 20). The miR-145 ASO may protect against demyelination during the peak and chronic phases of EAE. Representative TEM images show that there is extensive demyelination in the lumbar spinal cord of control ASO-treated mice during the peak and chronic phases of EAE (Figure 21). The miR-145 ASO-treated mice showed improvements in myelination with a significant increase in the number of myelinated axons. As previously mentioned, miR-145-5p inhibits OL differentiation through the downregulation of MYRF; therefore, inhibition of miR-145-5p with the ASO may allow for increased OL differentiation and increased remyelination (Letzen et al., 2010; Kornfeld et al., 2021). While we did not see increased *MYRF* mRNA expression following treatment with the miR-145 ASO (Figure 19), MYRF could be regulated post-transcriptionally or miR-145-5p inhibition could promote OL differentiation through another mechanism in our model. As well, the reduced inflammatory response following treatment with the miR-145 ASO may result in a reduced inflammatory attack against myelin and a subsequent reduction in demyelination. Together, these results suggest that the miR-145 ASO may promote remyelination and/or protect against demyelination in the CNS during EAE.

Inhibition of miR-145-5p with the ASO at the onset of EAE symptoms resulted in improvements in the clinical severity of EAE. The improvements are likely caused by a combination of reduced inflammation and improved myelination, demonstrating that miR-145-5p likely has a critical role in the regulation of inflammation and myelination.

4.4 Complete KO of miR-145 was more effective than ASO in protecting mice from EAE

Severity of EAE was improved with both the miR-145 KO and miR-145 ASO; however, there were differences in the effects of both methods (Kornfeld *et al*., unpublished). The overall clinical severity of EAE was reduced with the miR-145 KO and miR-145 ASO treatment. Both resulted in a reduction in the total number of days paralyzed, mean score at the chronic timepoint and instances of paralysis, but the miR-145 KO also resulted in delayed onset, reduced score at onset and delayed paralysis. The miR-145 KO mice showed greater improvements in clinical severity than the mice treated with the miR-145 ASO at the first instance of EAE.

Inflammation was reduced and myelination was improved with both the miR-145 KO and miR-145 ASO (Kornfeld *et al*., unpublished). While we did not see any significant alterations in the expression of cytokines *IFNγ*, *Il1β*, *Il6 and TNFα*, and chemokines *Ccl5* and *Cxcl1* in the spleen following miR-145 ASO treatment, there were some alterations following miR-145 KO. In the spinal cord, the miR-145 ASO resulted in a significant downregulation of *Il1β,* and trends towards upregulation of *IFNγ* at onset, downregulation of *Ccl5* at onset and upregulation of *Cxcl1* during the chronic phase. The miR-145 KO resulted in significant alterations in the expression of all cytokines and chemokines examined, especially during the onset phase of EAE. *Il1β* and *Ccl5* were also downregulated at EAE onset with the miR-145 KO, but IFNγ was downregulated and *Cxcl1* was upregulated at onset. The miR-145 KO and miR-145 ASO also both resulted in reduced cellular infiltration in the lumbar spinal cord. Cellular infiltration was decreased during the onset and chronic phases of EAE with the miR-145 KO, but just decreased during the chronic phase of EAE with the miR-145 ASO. There was a reduction in the number of

reactive astrocytes during the chronic phase of EAE with the miR-145 ASO. The miR-145 KO resulted in an increase in the number of reactive astrocytes during the onset and peak phases, but a decrease in the number of reactive astrocytes during the chronic phase of EAE. There was also a reduction in the number of reactive microglia during the chronic phase of EAE with the miR-145 ASO. The miR-145 KO resulted in an increase in the number of reactive microglia during the peak phase, but a reduction in the number of reactive microglia during the onset and chronic phases of EAE. Finally, myelination was improved with both the miR-145 KO and miR-145 ASO. The miR-145 ASO resulted in trends towards increased myelination area during the peak and chronic phases of EAE and the miR-145 KO resulted in a significant increase in myelination area during the onset and chronic phases of EAE.

Together, these results show that the miR-145 KO mice showed greater improvements in the severity of EAE compared to the mice treated with the miR-145 ASO. miR-145 KO resulted in improvements from the onset of EAE until the end of the study, whereas the miR-145 ASO only resulted in improvements in the later phase of EAE. The greater improvements are likely caused by the earlier timing of miR-145-5p inhibition and the larger reduction in miR-145-5p expression with the miR-145 KO.

4.5 Therapeutic Potential of miR-145-5p Inhibition

EAE is a mouse model used to study MS, particularly RRMS (Bjelobaba et al., 2018). EAE involves an immune response that starts in the periphery and travels to the CNS, resulting in neuroinflammation and demyelination. The immune attack leads to hind limb paralysis followed by partial recovery (Constantinescu et al., 2011; Kipp et al., 2017). Similar to EAE,

RRMS involves inflammatory attacks followed by remyelination resulting in cycles of clinical symptoms and partial/complete recovery (Dulamea, 2017; Franklin and Ffrench-Constant, 2017). In both EAE and RRMS, the degree of clinical symptoms directly reflects the extent of neuroinflammation and demyelination (Kipp et al., 2017). miR-145-5p has been shown to be overexpressed in people with RRMS compared to healthy controls (Keller et al., 2009; Tripathi et al., 2019). Overexpression of miR-145-5p inhibits OL differentiation, leading to impaired remyelination (Letzen et al., 2010; Kornfeld et al., 2021; Kornfeld *et al*., unpublished). Therefore, inhibition of miR-145-5p may improve remyelination capacity in RRMS.

Previous studies demonstrated that miR-145 KO resulted in improvements to the severity of EAE with a reduction in clinical severity, reduced neuroinflammation and increased myelination (Kornfeld *et al*., unpublished). Here, we show that miR-145-5p inhibition with a miR-145 ASO at the onset of symptoms also had a protective effect against EAE. The improvements in the severity of EAE following miR-145 KO and miR-145 ASO treatment suggest that miR-145-5p may represent a novel target in the treatment of RRMS.

ASOs have therapeutic potential because they bind specifically to the target RNA and knockdown its expression (Rinaldi and Wood, 2017; Bennett, 2019). In this study, the miR-145 ASO was delivered systemically, allowing us to examine the effects of miR-145-5p inhibition in the periphery and CNS. In humans, systemic delivery of a miR-145 ASO may be unfavorable to treat neurological disorders due to challenges associated with absorption and distribution of the ASO (Hammond et al., 2021). While we showed that the miR-145 ASO was able to enter the CNS following EAE induction, the miR-145 ASO likely would be unable to penetrate the BBB in a person with MS (Bennett et al., 2010). Direct injection of the ASO into the CNS would allow the

entry of the miR-145 ASO into the CNS. Intraventricular injection involves administration directly into the cerebrospinal fluid (CSF) of the cerebral ventricles and intrathecal injection involves administration directly into the subarachnoid space of the spinal cord (Glascock et al., 2011). While these methods would allow for immediate inhibition of miR-145-5p in the CNS, they are very invasive to the patient. Other potential mechanisms include nanoparticle and exosome-mediated delivery of the ASO into the CNS (Alvarez-Erviti et al., 2011; Fowler et al., 2020). Another consideration in the therapeutic potential of miR-145-5p is the off-target effects of its inhibition. miR-145-5p has been shown to be a tumour suppressor; therefore, its inhibition could lead to the proliferation and invasion of cancerous cells (Tang et al., 2019; Cao et al., 2020). Since miR-145-5p is ubiquitously expressed, caution should be taken with systemic miR-145-5p inhibition. Instead, methods to specifically target the MS lesions should be evaluated.

Inhibition of miR-145-5p has therapeutic potential in the EAE mouse model, suggesting that miR-145-5p may have therapeutic potential in MS. However, further research is needed to determine how to specifically target the CNS and avoid off-target effects.

4.6 Future Directions

Treatment with the miR-145 ASO was effective at improving the clinical severity of EAE. Here, we demonstrate that these improvements are likely caused by a reduction in neuroinflammation and improved myelination. Future studies should further elucidate the role of miR-145-5p in CNS inflammation and myelination. Multiple doses of miR-145 ASO should also be tested. We would like to investigate the regulation of NFκB, Twist2 and Nurr1 by miR-

145-5p. We would also like to further investigate the effects of miR-145-5p inhibition on the regulation of MYRF and other factors involved in OL differentiation. Finally, we would like to investigate the effect of miR-145 ASO treatment in the chronic cuprizone model to determine if inhibition of miR-145-5p can promote remyelination and has therapeutic potential in progressive forms of MS.

5. Conclusion

In this study, we demonstrated that an ASO can be used to knockdown miR-145-5p in the EAE mouse model. Treatment with the miR-145 ASO at the first instance of the disease resulted in improved clinical severity of EAE, as seen with significant reductions in the overall EAE score during the later phase of the disease, the number of days paralyzed, the score at the chronic timepoint and the number of instances of paralysis. These improvements coincided with improvements in neuroinflammation and myelination. This study supports previous work by our lab which showed that miR-145 KO improved the clinical severity of EAE, reduced inflammation and increased myelination. Together, our results demonstrate that miR-145-5p inhibition represents a novel therapeutic target in the treatment of MS.

References

Al-Shamsi M, Shahin A, Ibrahim MF, Tareq S, Souid AK, Mensah-Brown EPK (2015) Bioenergetics of the spinal cord in experimental autoimmune encephalitis of rats. BMC Neurosci 16.

Alfredsson L, Olsson T (2019) Lifestyle and Environmental Factors in Multiple Sclerosis. Cold Spring Harb Perspect Med 9:a028944.

Alvarez-Erviti L, Seow Y, Yin H, Betts C, Lakhal S, Wood MJA (2011) Delivery of siRNA to the mouse brain by systemic injection of targeted exosomes. Nat Biotechnol 2011 294 29:341–345.

Bajan S, Hutvagner G (2020) RNA-Based Therapeutics: From Antisense Oligonucleotides to miRNAs. Cells 9.

Baldassari LE, Fox RJ (2018) Therapeutic Advances and Challenges in the Treatment of Progressive Multiple Sclerosis. Drugs 78:1549–1566.

Bennett CF (2019) Therapeutic Antisense Oligonucleotides Are Coming of Age. Annu Rev Med 70:307–321.

Bennett J, Basivireddy J, Kollar A, Biron KE, Reickmann P, Jefferies WA, McQuaid S (2010) Blood-brain barrier disruption and enhanced vascular permeability in the multiple sclerosis model EAE. J Neuroimmunol 229:180–191.

Bjelobaba I, Begovic-Kupresanin V, Pekovic S, Lavrnja I (2018) Animal models of multiple sclerosis: Focus on experimental autoimmune encephalomyelitis. J Neurosci Res 96:1021–1042.

Borbet TC, Hines MJ, Koralov SB (2021) MicroRNA regulation of B cell receptor signaling. Immunol Rev 304:111–125.

Boyd A, Zhang H, Williams A (2013) Insufficient OPC migration into demyelinated lesions is a cause of poor remyelination in MS and mouse models. Acta Neuropathol 125:841.

Brambilla R (2019) The contribution of astrocytes to the neuroinflammatory response in multiple sclerosis and experimental autoimmune encephalomyelitis. Acta Neuropathol 137:757.

Brambilla R, Persaud T, Hu X, Karmally S, Shestopalov VI, Dvoriantchikova G, Ivanov D, Nathanson L, Barnum SR, Bethea JR (2009) Transgenic Inhibition of Astroglial NF-κB Improves Functional Outcome in Experimental Autoimmune Encephalomyelitis by Suppressing Chronic Central Nervous System Inflammation. J Immunol 182:2628.

Brandão WN, De Oliveira MG, Andreoni RT, Nakaya H, Farias AS, Peron JPS (2020) Neuroinflammation at single cell level: What is new? J Leukoc Biol 108:1129–1137.

Broderick JA, Zamore PD (2011) MicroRNA therapeutics. Gene Ther 18:1104–1110.

Bross M, Hackett M, Bernitsas E (2020) Approved and Emerging Disease Modifying Therapies on Neurodegeneration in Multiple Sclerosis. Int J Mol Sci 21:1–15.

Buller B, Chopp M, Ueno Y, Zhang L, Zhang RL, Morris D, Zhang Y, Zhang ZG (2012) Regulation of serum response factor by miRNA-200 and miRNA-9 modulates oligodendrocyte progenitor cell differentiation. Glia 60:1906.

Cao H, Pan G, Tang S, Zhong N, Liu H, Zhou H, Peng Q, Zou Y (2020) miR-145-5p Regulates the Proliferation, Migration and Invasion in Cervical Carcinoma by Targeting KLF5. Onco Targets Ther 13:2369.

Catalanotto C, Cogoni C, Zardo G (2016) MicroRNA in Control of Gene Expression: An Overview of Nuclear Functions. Int J Mol Sci 17:1712.

Charles P, Reynolds R, Seilhean D, Rougon G, Aigrot MS, Niezgoda A, Zalc B, Lubetzki C (2002) Re-expression of PSA-NCAM by demyelinated axons: an inhibitor of remyelination in multiple sclerosis? Brain 125:1972–1979.

Chastain EML, Duncan DS, Rodgers JM, Miller SD (2011) The Role of Antigen Presenting Cells in Multiple Sclerosis. Biochim Biophys Acta 1812:265.

Chen D, Farwell MA, Zhang B (2010) MicroRNA as a new player in the cell cycle. J Cell Physiol 225:296–301.

Chu F, Shi M, Zheng C, Shen D, Zhu J, Zheng X, Cui L (2018) The roles of macrophages and microglia in multiple sclerosis and experimental autoimmune encephalomyelitis. J Neuroimmunol 318:1–7.

Cobb BS, Nesterova TB, Thompson E, Hertweck A, O'Connor E, Godwin J, Wilson CB, Brockdorff N, Fisher AG, Smale ST, Merkenschlager M (2005) T cell lineage choice and differentiation in the absence of the RNase III enzyme Dicer. J Exp Med 201:1367–1373.

Constantinescu CS, Farooqi N, O'Brien K, Gran B (2011) Experimental autoimmune encephalomyelitis (EAE) as a model for multiple sclerosis (MS). Br J Pharmacol 164:1079.

Correale J, Gaitán MI, Ysrraelit MC, Fiol MP (2016) Progressive multiple sclerosis: from pathogenic mechanisms to treatment. Brain 140:527–546.

Cunniffe N, Coles A (2021) Promoting remyelination in multiple sclerosis. J Neurol 268:30.

de Faria Jr O, Moore CS, Kennedy TE, Antel JP, Bar-Or A, Dhaunchak AS (2012) MicroRNA dysregulation in multiple sclerosis. Front Genet 3:311.

Dendrou CA, Fugger L, Friese MA (2015) Immunopathology of multiple sclerosis. Nat Rev Immunol 15:545–558.

Dhuri K, Bechtold C, Quijano E, Pham H, Gupta A, Vikram A, Bahal R (2020) Antisense Oligonucleotides: An Emerging Area in Drug Discovery and Development. J Clin Med 9:1–24.

Dos Santos AC, Barsante MM, Esteves Arantes RM, Bernard CCA, Teixeira MM, Carvalho-Tavares J (2005) CCL2 and CCL5 mediate leukocyte adhesion in experimental autoimmune encephalomyelitis—an intravital microscopy study. J Neuroimmunol 162:122–129.

Duan S, Lv Z, Fan X, Wang L, Han F, Wang H, Bi S (2014) Vitamin D status and the risk of multiple sclerosis: A systematic review and meta-analysis. Neurosci Lett 570:108–113.

Dugas JC, Cuellar TL, Scholze A, Ason B, Ibrahim A, Emery B, Zamanian JL, Foo LC, McManus MT, Barres BA (2010) Dicer1 and miR-219 Are required for normal oligodendrocyte differentiation and myelination. Neuron 65:597–611.

Dulamea AO (2017) The contribution of oligodendrocytes and oligodendrocyte progenitor cells to central nervous system repair in multiple sclerosis: perspectives for remyelination therapeutic strategies. Neural Regen Res 12:1939–1944.

El-behi M, Rostami A, Ciric B (2010) Current Views on the Roles of Th1 and Th17 Cells in Experimental Autoimmune Encephalomyelitis. J Neuroimmune Pharmacol 5:189.

Emery B, Agalliu D, Cahoy JD, Watkins TA, Dugas JC, Mulinyawe SB, Ibrahim A, Ligon KL, Rowitch DH, Barres BA (2009) Identification of Myelin-gene Regulatory Factor as a Critical Transcriptional Regulator Required for CNS Myelination. Cell 138:172.

Ettle B, Schlachetzki JCM, Winkler J (2016) Oligodendroglia and Myelin in Neurodegenerative Diseases: More Than Just Bystanders? Mol Neurobiol 53:3046–3062.

Faissner S, Plemel JR, Gold R, Yong VW (2019) Progressive multiple sclerosis: from

pathophysiology to therapeutic strategies. Nat Rev Drug Discov 2019 1812 18:905–922.

Fowler MJ, Cotter JD, Knight BE, Sevick-Muraca EM, Sandberg DI, Sirianni RW (2020) Intrathecal Drug Delivery in the Era of Nanomedicine. Adv Drug Deliv Rev 165–166:77.

Franklin RJM (2002) Why does remyelination fail in multiple sclerosis? Nat Rev Neurosci 3:705–714.

Franklin RJM, Ffrench-Constant C (2008) Remyelination in the CNS: from biology to therapy. Nat Rev Neurosci 9:839–855.

Franklin RJM, Ffrench-Constant C (2017) Regenerating CNS myelin - From mechanisms to experimental medicines. Nat Rev Neurosci 18:753–769.

Frazier KS (2015) Antisense Oligonucleotide Therapies: The Promise and the Challenges from a Toxicologic Pathologist's Perspective. Toxicol Pathol 43:78–89.

Galloway DA, Gowing E, Setayeshgar S, Kothary R (2019) Inhibitory milieu at the multiple sclerosis lesion site and the challenges for remyelination. Glia 68:859–877.

Galloway DA, Moore CS (2016) MiRNAs as emerging regulators of oligodendrocyte development and differentiation. Front Cell Dev Biol 4:59.

Gholamzad M, Ebtekar M, Ardestani MS, Azimi M, Mahmodi Z, Mousavi MJ, Aslani S (2018) A comprehensive review on the treatment approaches of multiple sclerosis: currently and in the future. Inflamm Res 2018 681 68:25–38.

Gilmour H, Ramage-Morin PL, Wong SL (2018) Multiple sclerosis: Prevalence and impact. Heal Rep 29:3–8.

Glascock JJ, Osman EY, Coady TH, Rose FF, Shababi M, Lorson CL (2011) Delivery of Therapeutic Agents Through Intracerebroventricular (ICV) and Intravenous (IV) Injection in Mice. J Vis

Exp 56:2968.

Golden LC, Voskuhl R (2017) The Importance of Studying Sex Differences in Disease: The Example of Multiple Sclerosis. J Neurosci Res 95:633.

Gonzalez-Perez O, Alvarez-Buylla A (2011) Oligodendrogenesis in the subventricular zone and the role of epidermal growth factor. Brain Res Rev 67:147.

Government of Canada (2018) Multiple Sclerosis In Canada. Available at: https://www.canada.ca/en/public-health/services/publications/diseases-conditions/multiple-sclerosis-infographic.html [Accessed September 10, 2021].

Gruchot J, Weyers V, Göttle P, Förster M, Hartung H-P, Küry P, Kremer D (2019) The Molecular Basis for Remyelination Failure in Multiple Sclerosis. Cells 8:825.

Gu SM, Park MH, Yun HM, Han SB, Oh KW, Son DJ, Yun JS, Hong JT (2016) CCR5 knockout suppresses experimental autoimmune encephalomyelitis in C57BL/6 mice. Oncotarget 7:15382.

Hammond SM et al. (2021) Delivery of oligonucleotide-based therapeutics: challenges and opportunities. EMBO Mol Med 13:e13243.

Han H, Myllykoski M, Ruskamo S, Wang C, Kursula P (2013) Myelin-specific proteins: A structurally diverse group of membrane-interacting molecules. BioFactors 39:233–241.

Harlow DE, Macklin WB (2014) Inhibitors of myelination: ECM changes, CSPGs andPTPs. Exp Neurol 251:39.

Hauptmann J et al. (2020) Interleukin-1 promotes autoimmune neuroinflammation by suppressing endothelial heme oxygenase-1 at the blood–brain barrier. Acta Neuropathol 140:549.

Hauser SL, Cree BA (2020) Treatment of Multiple Sclerosis: A Review. Am J Med 133:1380-1390.e2.

Hedström AK, Olsson T, Alfredsson L (2012) High body mass index before age 20 is associated with increased risk for multiple sclerosis in both men and women: Mult Scler 18:1334–1336.

Hemmer B, Kerschensteiner M, Korn T (2015) Role of the innate and adaptive immune responses in the course of multiple sclerosis. Lancet Neurol 14:406–419.

Hinks GL, Franklin RJM (1999) Distinctive Patterns of PDGF-A, FGF-2, IGF-I, and TGF-b1 Gene Expression during Remyelination of Experimentally-Induced Spinal Cord Demyelination.

Hollenbach JA, Oksenberg JR (2015) The Immunogenetics of Multiple Sclerosis: A Comprehensive Review. J Autoimmun 64:13.

Hooke Laboratories (2008) EAE Induction by Active Immunization in C57BL/6 Mice. In: Hooke Kit Protocols, pp 1–24. Lawrence, MA, USA.

Huang W-J, Chen W-W, Zhang X (2017) Multiple sclerosis: Pathology, diagnosis and treatments. Exp Ther Med 13:3163.

Jacobs BM, Giovannoni G, Cuzick J, Dobson R (2020) Systematic review and meta-analysis of the association between Epstein–Barr virus, multiple sclerosis and other risk factors. Mult Scler 26:1281.

Jeker LT, Bluestone JA (2013) microRNA regulation of T-cell differentiation and function. Immunol Rev 253:65.

Junker A, Krumbholz M, Eisele S, Mohan H, Augstein F, Bittner R, Lassmann H, Wekerle H, Hohlfeld R, Meinl E (2009) MicroRNA profiling of multiple sclerosis lesions identifies

modulators of the regulatory protein CD47. Brain 132:3342–3352.

Juźwik CA, S. Drake S, Zhang Y, Paradis-Isler N, Sylvester A, Amar-Zifkin A, Douglas C, Morquette B, Moore CS, Fournier AE (2019) microRNA dysregulation in neurodegenerative diseases: A systematic review. Prog Neurobiol 182:101664.

Karpus WJ (2020) Cytokines and Chemokines in the Pathogenesis of Experimental Autoimmune Encephalomyelitis. J Immunol 204:316–326.

Katz Sand I (2015) Classification, diagnosis, and differential diagnosis of multiple sclerosis. Curr Opin Neurol 28:193–205.

Kawase-Koga Y, Otaegi G, Sun T (2009) Different timings of Dicer deletion affect neurogenesis and gliogenesis in the developing mouse central nervous system. Dev Dyn 238:2800.

Keller A, Leidinger P, Lange J, Borries A, Schroers H, Scheffler M, Lenhof H-P, Ruprecht K, Meese E (2009) Multiple Sclerosis: MicroRNA Expression Profiles Accurately Differentiate Patients with Relapsing-Remitting Disease from Healthy Controls. PLoS One 4:e7440.

Kim VN (2005) MicroRNA biogenesis: coordinated cropping and dicing. Nat Rev Mol Cell Biol 6:376–385.

Kipp M, Nyamoya S, Hochstrasser T, Amor S (2017) Multiple sclerosis animal models: a clinical and histopathological perspective. Brain Pathol 27:123–137.

Koralov SB, Muljo SA, Galler GR, Krek A, Chakraborty T, Kanellopoulou C, Jensen K, Cobb BS, Merkenschlager M, Rajewsky N, Rajewsky K (2008) Dicer Ablation Affects Antibody Diversity and Cell Survival in the B Lymphocyte Lineage. Cell 132:860–874.

Kornfeld SF, Cummings SE, Fathi S, Bonin SR, Kothary R (2021) MiRNA-145-5p prevents differentiation of oligodendrocyte progenitor cells by regulating expression of myelin gene

regulatory factor. J Cell Physiol 236:997–1012.

Kornfeld SF, Kothary R (2020) MiR-145-5p: Its Roles in Oligodendrocyte Differentiation and Its Contributions to the Pathophysiology of Demyelinating Disease.

Krol J, Loedige I, Filipowicz W (2010) The widespread regulation of microRNA biogenesis, function and decay. Nat Rev Genet 11:597–610.

Kuhn S, Gritti L, Crooks D, Dombrowski Y (2019) Oligodendrocytes in Development, Myelin Generation and Beyond. Cells 8:1424.

Langelaar J van, Rijvers L, Smolders J, Luijn MM van (2020) B and T Cells Driving Multiple Sclerosis: Identity, Mechanisms and Potential Triggers. Front Immunol 11:760.

Lau P, Verrier JD, Nielsen JA, Johnson KR, Notterpek L, Hudson LD (2008) Identification of Dynamically Regulated MicroRNA and mRNA Networks in Developing Oligodendrocytes. J Neurosci 28:11720.

Lawrence T (2009) The Nuclear Factor NF-κB Pathway in Inflammation. Cold Spring Harb Perspect Biol 1:a001651.

Lecca D, Marangon D, Coppolino GT, Méndez AM, Finardi A, Costa GD, Martinelli V, Furlan R, Abbracchio MP (2016) MiR-125a-3p timely inhibits oligodendroglial maturation and is pathologically up-regulated in human multiple sclerosis. Sci Rep 6:34503.

Lemus HN, Warrington AE, Rodriguez M (2018) Multiple Sclerosis: Mechanisms of Disease and Strategies for Myelin and Axonal Repair. Neurol Clin 36:1.

Letzen BS, Liu C, Thakor N V., Gearhart JD, All AH, Kerr CL (2010) MicroRNA Expression Profiling of Oligodendrocyte Differentiation from Human Embryonic Stem Cells. PLoS One 5:e10480.

Li D, Liu X, Liu T, Liu H, Tong L, Jia S, Wang YF (2020) Neurochemical regulation of the expression

and function of glial fibrillary acidic protein in astrocytes. Glia 68:878–897.

Li F, Zhou M-W, Liu N, Yang Y-Y, Xing H-Y, Lu Y, Liu X-X (2019) MicroRNA-219 Inhibits Proliferation and Induces Differentiation of Oligodendrocyte Precursor Cells after Contusion Spinal Cord Injury in Rats. Neural Plast 2019:9610687.

Li JS, Yao ZX (2012) MicroRNAs: Novel regulators of oligodendrocyte differentiation and potential therapeutic targets in demyelination-related diseases. Mol Neurobiol 45:200–212.

Lin S-T, Fu Y-H (2009) miR-23 regulation of lamin B1 is crucial for oligodendrocyte development and myelination. Dis Model Mech 2:178.

Lubetzki C, Zalc B, Williams A, Stadelmann C, Stankoff B (2020) Remyelination in multiple sclerosis: from basic science to clinical translation. Lancet Neurol 19:678–688.

Lynam-Lennon N, Maher SG, Reynolds J V. (2009) The roles of microRNA in cancer and apoptosis. Biol Rev 84:55–71.

Mahesh G, Biswas R (2019) MicroRNA-155: A Master Regulator of Inflammation. J Interf Cytokine Res 39:321.

Matsuki T, Nakae S, Sudo K, Horai R, Iwakura Y (2006) Abnormal T cell activation caused by the imbalance of the IL-1/IL-1R antagonist system is responsible for the development of experimental autoimmune encephalomyelitis. Int Immunol 18:399–407.

Matsuyama H, Suzuki HI (2020) Systems and Synthetic microRNA Biology: From Biogenesis to Disease Pathogenesis. Int J Mol Sci 21:132.

Mi S et al. (2007) LINGO-1 antagonist promotes spinal cord remyelination and axonal integrity in MOG-induced experimental autoimmune encephalomyelitis. Nat Med 2007 1310

13:1228–1233.

Michalski J-P, Kothary R (2015) Oligodendrocytes in a Nutshell. Front Cell Neurosci 9:340.

Michel L, Touil H, Pikor NB, Gommerman JL, Prat A, Bar-Or A (2015) B Cells in the Multiple Sclerosis Central Nervous System: Trafficking and Contribution to CNS-Compartmentalized Inflammation. Front Immunol 6:636.

Mohr AM, Mott JL (2015) Overview of microRNA biology. Semin Liver Dis 35:3–11.

MS Society of Canada (2021) Treatments — MS Society of Canada. Available at: https://mssociety.ca/managing-ms/treatments [Accessed October 28, 2021].

Muljo SA, Ansel KM, Kanellopoulou C, Livingston DM, Rao A, Rajewsky K (2005) Aberrant T cell differentiation in the absence of Dicer. J Exp Med 202:261–269.

Murugaiyan G, Beynon V, Mittal A, Joller N, Weiner HL (2011) Silencing MicroRNA-155 Ameliorates Experimental Autoimmune Encephalomyelitis. J Immunol 187:2213.

Noseworthy JH, Lucchinetti C, Rodriguez M, Weinshenker BG (2009) Multiple Sclerosis. N Engl J Med 343:938–952.

O'Connell RM, Kahn D, Gibson WSJ, Round JL, Scholz RL, Chaudhuri AA, Kahn ME, Rao DS, Baltimore D (2010) MicroRNA-155 promotes autoimmune inflammation by enhancing inflammatory T cell development. Immunity 33:607.

O'Gorman C, Lin R, Stankovich J, Broadley SA (2013) Modelling Genetic Susceptibility to Multiple Sclerosis with Family Data. Neuroepidemiology 40:1–12.

Ohsawa K, Imai Y, Sasaki Y, Kohsaka S (2004) Microglia/macrophage-specific protein Iba1 binds to fimbrin and enhances its actin-bundling activity. J Neurochem 88:844–856.

Orton SM, Herrera BM, Yee IM, Valdar W, Ramagopalan S V., Sadovnick AD, Ebers GC (2006)

Sex ratio of multiple sclerosis in Canada: a longitudinal study. Lancet Neurol 5:932–936.

Ostkamp P et al. (2021) Sunlight exposure exerts immunomodulatory effects to reduce multiple sclerosis severity. Proc Natl Acad Sci U S A 118:e2018457118.

Otaegui D, Baranzini SE, Armañanzas R, Calvo B, Muñoz-Culla M, Khankhanian P, Inza I, Lozano JA, Castillo-Triviño T, Asensio A, Olaskoaga J, Lopez de Munain A (2009) Differential Micro RNA Expression in PBMC from Multiple Sclerosis Patients. PLoS One 4:e6309.

Patel J, Balabanov R (2012) Molecular Mechanisms of Oligodendrocyte Injury in Multiple Sclerosis and Experimental Autoimmune Encephalomyelitis. Int J Mol Sci 13:10647.

Pierson ER, Wagner CA, Goverman JM (2018) The contribution of neutrophils to CNS autoimmunity. Clin Immunol 189:23.

Rinaldi C, Wood MJA (2017) Antisense oligonucleotides: the next frontier for treatment of neurological disorders. Nat Rev Neurol 14:9–21.

Robinson AP, Harp CT, Noronha A, Miller SD (2014) The experimental autoimmune encephalomyelitis (EAE) model of MS: utility for understanding disease pathophysiology and treatment. Handb Clin Neurol 122:173–189.

Ruggieri S, Tortorella C, Gasperini C (2017) Anti lingo 1 (opicinumab) a new monoclonal antibody tested in relapsing remitting multiple sclerosis. http://dx.doi.org.proxy.bib.uottawa.ca/101080/1473717520171378098 17:1081–1089.

Saliminejad K, Khorshid HRK, Fard SS, Ghaffari SH (2019) An overview of microRNAs: Biology, functions, therapeutics, and analysis methods. J Cell Physiol 234:5451–5465.

Shi Y, Jin Y (2009) MicroRNA in cell differentiation and development. Sci China Ser C Life Sci 52:205–211.

Shin D, Shin J-Y, McManus MT, Ptáček LJ, Fu Y-H (2009) Dicer Ablation in Oligodendrocytes Provokes Neuronal Impairment in Mice. Ann Neurol 66:843.

Sievers C, Meira M, Hoffmann F, Fontoura P, Kappos L, Lindberg RLP (2012) Altered microRNA expression in B lymphocytes in multiple sclerosis: Towards a better understanding of treatment effects. Clin Immunol 144:70–79.

Simpson S, Blizzard L, Otahal P, Mei I Van der, Taylor B (2011) Latitude is significantly associated with the prevalence of multiple sclerosis: a meta-analysis. J Neurol Neurosurg Psychiatry 82:1132–1141.

Stoolman JS, Duncker PC, Huber AK, Giles DA, Washnock-Schmid JM, Soulika AM, Segal BM (2018) An IFNγ/CXCL2 regulatory pathway determines lesion localization during EAE. J Neuroinflammation 15:208.

Su W, Hopkins S, Nesser NK, Sopher B, Silvestroni A, Ammanuel S, Jayadev S, Möller T, Weinstein J, Garden GA (2014) The p53 transcription factor modulates microglia behavior through microRNA dependent regulation of c-Maf. J Immunol 192:358.

Sun P, Liu DZ, Jickling GC, Sharp FR, Yin KJ (2018) MicroRNA-based therapeutics in central nervous system injuries. J Cereb Blood Flow Metab 38:1125.

Sutton CE, Lalor SJ, Sweeney CM, Brereton CF, Lavelle EC, Mills KHG (2009) Interleukin-1 and IL-23 Induce Innate IL-17 Production from γδ T Cells, Amplifying Th17 Responses and Autoimmunity. Immunity 31:331–341.

Tang W, Zhang X, Tan W, Gao J, Pan L, Ye X, Chen L, Zheng W (2019) miR-145-5p Suppresses Breast Cancer Progression by Inhibiting SOX2. J Surg Res 236:278–287.

Tiane A, Schepers M, Rombaut B, Hupperts R, Prickaerts J, Hellings N, Hove D van den,

Vanmierlo T (2019) From OPC to Oligodendrocyte: An Epigenetic Journey. Cells 8:1236.

Tripathi A, Volsko C, Datta U, Regev K, Dutta R (2019) Expression of disease-related miRNAs in white-matter lesions of progressive multiple sclerosis brains. Ann Clin Transl Neurol 6:854.

Vora P, Pillai P, Mustapha J, Kowal C, Shaffer S, Bose R, Namaka M, Frost EE (2012) CXCL1 regulation of oligodendrocyte progenitor cell migration is independent of calcium signaling. Exp Neurol 236:259–267.

Walton C, King R, Rechtman L, Kaye W, Leray E, Marrie RA, Robertson N, Rocca N La, Uitdehaag B, Mei I van der, Wallin M, Helme A, Napier CA, Rijke N, Baneke P (2020) Rising prevalence of multiple sclerosis worldwide: Insights from the Atlas of MS, third edition. Mult Scler 26:1816.

Wang D, Lu Z, Zhang H, Jin SF, Yang H, Li YM, Shi LY (2016) Daphnetin Alleviates Experimental Autoimmune Encephalomyelitis via Regulating Dendritic Cell Activity. CNS Neurosci Ther 22:558.

Wang X, Tang K, Wang Y, Chen Y, Yang M, Gu C, Wang J, Wang Y, Yuan Y (2019) Elevated microRNA-145-5p increases matrix metalloproteinase-9 by activating the nuclear factor-κB pathway in rheumatoid arthritis. Mol Med Rep 20:2703.

Watson AES, Goodkey K, Footz T, Voronova A (2020) Regulation of CNS precursor function by neuronal chemokines. Neurosci Lett 715:134533.

Winter J, Jung S, Keller S, Gregory RI, Diederichs S (2009) Many roads to maturity: microRNA biogenesis pathways and their regulation. Nat Cell Biol 11:228–234.

Wu T, Wieland A, Araki K, Davis CW, Ye L, Hale JS, Ahmed R (2012) Temporal expression of microRNA cluster miR-17-92 regulates effector and memory CD8 + T-cell differentiation.

Proc Natl Acad Sci U S A 109:9965–9970.

Xie X, Peng L, Zhu J, Zhou Y, Li L, Chen Y, Yu S, Zhao Y (2017) miR-145-5p/Nurr1/TNF-α Signaling-Induced Microglia Activation Regulates Neuron Injury of Acute Cerebral Ischemic/Reperfusion in Rats. Front Mol Neurosci 10:383.

Ysrraelit MC, Correale J (2019) Impact of sex hormones on immune function and multiple sclerosis development. Immunology 156:9.

Zhang D, Qiao L, Fu T (2020) Paricalcitol improves experimental autoimmune encephalomyelitis (EAE) by suppressing inflammation via NF-κB signaling. Biomed Pharmacother 125:109528.

Zhang J, Zhang ZG, Lu M, Zhang Y, Shang X, Chopp M (2019) MiR-146a promotes oligodendrocyte progenitor cell differentiation and enhances remyelination in a model of experimental autoimmune encephalomyelitis. Neurobiol Dis 125:154–162.

Zhang Y, Argaw AT, Gurfein BT, Zameer A, Snyder BJ, Ge C, Lu QR, Rowitch DH, Raine CS, Brosnan CF, John GR (2009) Notch1 signaling plays a role in regulating precursor differentiation during CNS remyelination. Proc Natl Acad Sci U S A 106:19162.

Zhou X, Liu X, Liu L, Han C, Xie Z, Liu X, Xu Y, Li F, Bi J, Zheng C (2020) Transplantation of IFN-γ Primed hUCMSCs Significantly Improved Outcomes of Experimental Autoimmune Encephalomyelitis in a Mouse Model. Neurochem Res 45:1510–1517.

Zuchero JB, Barres BA (2013) Intrinsic and extrinsic control of oligodendrocyte development. Curr Opin Neurobiol 23:914.